

Three Time-Scales In An Extended Bonhoeffer–Van Der Pol Oscillator

P. De Maesschalck · E. Kutafina · N. Popović

Received: 17 August 2013 / Revised: 15 February 2014 / Published online: 18 March 2014
© Springer Science+Business Media New York 2014

Abstract We consider an extended three-dimensional Bonhoeffer–van der Pol oscillator which generalises the planar FitzHugh–Nagumo model from mathematical neuroscience, and which was recently studied by Sekikawa et al. (Phys Lett A 374(36):3745–3751, 2010) and by Freire and Gallas (Phys Lett A 375:1097–1103, 2011). Focussing on a parameter regime which has hitherto been neglected, and in which the governing equations evolve on three distinct time-scales, we propose a reduction to a model problem that was formulated by Krupa et al. (J Appl Dyn Syst 7(2):361–420, 2008) as a canonical form for such systems. Based on results previously obtained in Krupa et al. (2008), we characterise completely the mixed-mode dynamics of the resulting three time-scale extended Bonhoeffer–van der Pol oscillator from the point of view of geometric singular perturbation theory, thus complementing the findings reported in Sekikawa et al. (2010). In particular, we specify in detail the mixed-mode patterns that are observed upon variation of a bifurcation parameter which is naturally obtained by combining two of the original parameters in the system, and we derive asymptotic estimates for the corresponding parameter intervals. We thereby also disprove a conjecture of Tu (SIAM J Appl Math 49(2): 331–343, 1989), where it was postulated that no stable periodic orbits of mixed-mode type can be observed in an equivalent extension of the Bonhoeffer–van der Pol equations.

Keywords Bonhoeffer–van der Pol oscillator · Mixed-mode oscillations · Canards · Geometric singular perturbation theory · Blow-up technique

P. De Maesschalck · E. Kutafina
Hasselt University, Campus Diepenbeek, Agoralaan Gebouw D, 3590 Diepenbeek, Belgium
e-mail: Peter.DeMaesschalck@uhasselt.be

E. Kutafina
AGH University of Science and Technology, al. Mickiewicza 30, 30-059 Kraków, Poland
e-mail: Ekaterina.Kutafina@uhasselt.be

N. Popović (✉)
School of Mathematics and Maxwell Institute for Mathematical Sciences, University of Edinburgh, James Clerk Maxwell Building, King's Buildings, Mayfield Road, Edinburgh EH9 3JZ, UK
e-mail: Nikola.Popovic@ed.ac.uk

Mathematics Subject Classification (2010) 34D15 · 34E13 · 34E17 · 34E20 · 34C26 · 37G15

1 Introduction

In this article, we consider the three-dimensional Bonhoeffer–van der Pol oscillator, a known extension of the classical planar FitzHugh–Nagumo equations from mathematical neuroscience [9], which was studied most recently by Sekikawa et al. [17] and by Freire and Gallas [7]. Specifically, we are concerned with the following system of equations:

$$\varepsilon \dot{x} = x(1 - x^2) + y + z, \quad (1a)$$

$$\dot{y} = -x - k_1 y + B_0, \quad (1b)$$

$$\dot{z} = k_3(-x - k_1 z + B_0); \quad (1c)$$

here, we have retained the notation of [17], with ε the ‘small’ singular perturbation parameter and three additional parameters which are denoted by B_0 , k_1 , and k_3 .

Equation (1) is known to display rich dynamics on at least two different time-scales due to the presence of the small parameter ε [7, 17]. Here, we focus on the stable mixed-mode oscillatory behaviour [3] that was reported both numerically and experimentally—by construction of an equivalent electrical circuit—in [17]; in the follow-up article [7], the resulting mixed-mode patterns were organised systematically in terms of Farey trees, as well as of more general Stern–Brocot trees. In both studies, the two parameters B_0 and k_3 were identified as crucial for the unfolding of the bifurcation structure of (1); in particular, Sekikawa et al. [17] observed mixed-mode dynamics close to a pair of (supercritical) Hopf bifurcations which occur in (1) for $B_0 \approx \pm \frac{1}{2}$, where, additionally, k_3 was assumed to be close to one. (We note that there is a symmetry $(x, y, z, B_0) \rightarrow (-x, -y, -z, -B_0)$ in Eq. (1), allowing us to restrict our study to the regime where $B_0 > 0$ or, rather, to consider $B_0 \approx \frac{1}{2}$ only.) Mixed-mode oscillations (MMOs) are typically found in dynamical systems that evolve on multiple scales, and that are hence ‘fast-slow;’ see [3] and the references therein for details. Due to the oftentimes complex nature of these systems, the presence of MMOs is frequently established only numerically; almost equally often, it is proven by applying geometric singular perturbation theory [6, 10]. The latter approach crucially relies on a separation of scales to achieve a (partial) dimension reduction, thus allowing for a semi-analytical treatment in many cases. One downside of the geometric approach, however, is that, strictly speaking, it is only valid in the limit as $\varepsilon \rightarrow 0$, where ε defines the scale separation in the system. Fortunately, the analysis frequently does extend to ‘reasonable’ values of $\varepsilon > 0$; in fact, numerical evidence presented in Sect. 4 below suggests that the results obtained in this article may remain valid for ‘moderately large’ $\varepsilon (=0.1)$.

Our aim here is to analyse Eq. (1) from the point of view of geometric singular perturbation theory, focussing on a parameter regime that has not been considered in previous work [7, 17]: we will show that, for $0 \lesssim k_3 \ll 1$, Eq. (1) evolves on three distinct time-scales, and we will describe in detail the corresponding mixed-mode dynamics, thus complementing the findings of Sekikawa et al. [17]. Specifically, it follows from (1c) that z is a ‘super-slow’ variable then; in fact, in the limit of $k_3 = 0$, z is constant, i.e., the system reduces to a van der Pol-like oscillator that can undergo a ‘classical’ canard explosion [5, 12], transitioning from a stable equilibrium to relaxation oscillation via a family of canard cycles as z is varied. (Similarly, a reduction to a planar FitzHugh–Nagumo system is feasible when $k_3 = 1$: after introduction of $y + z$ as a new variable, it becomes apparent that the $(x, y + z)$ -equations

decouple.) It is hence reasonable to assume that a canard phenomenon underlies the mixed-mode dynamics which is generated by Eq. (1) when k_3 is non-zero, but small. In fact, the so-called ‘generalised canard mechanism’ [1] has been proposed as a unified generating mechanism for mixed-mode behaviour in singularly perturbed systems of equations such as (1): typically, MMOs are characterised by an alternation of small-amplitude oscillations (SAOs) that are followed by large excursions, or large-amplitude oscillations (LAOs). The former can frequently be shown to be due to (local) flow past a canard point, while the latter can be described by a (global) relaxation-like return mechanism. Periodic mixed-mode type orbits consisting of k SAOs and L LAOs are identified with the signature L^k ; knowledge of the possible signatures in a given system, in combination with estimates for the relevant parameter intervals, characterises completely the mixed-mode dynamics of the system.

In our case, with $0 \lesssim k_3 \ll 1$, such a characterisation is conveniently achieved by reducing Eq. (1) to the simplified three time-scale model

$$\varepsilon \dot{v} = -z + f_2 v^2 + f_3 v^3, \tag{2a}$$

$$\dot{z} = v - w, \tag{2b}$$

$$\dot{w} = \varepsilon(\mu - g_1 z), \tag{2c}$$

which was proposed in [14] as representative for that type of system. Here, f_2 , f_3 , and g_1 denote fixed parameters, ε is assumed to be a small parameter, as above, and μ is the bifurcation parameter that unfolds the mixed-mode dynamics of (2).

While no comprehensive theory exists for perturbative scenarios that involve more than one singular parameter, in the seminal article [14], Krupa et al. characterised the mixed-mode dynamics that is generated by Eq. (2). The authors then argued that their model is prototypical, in that it reflects the dynamical properties of three time-scale systems with similar local structure, as described in their article. While the analysis of [14] does not translate verbatim to the context of the extended Bonhoeffer–van der Pol oscillator, Eq. (1), as we encounter additional terms in the reduced equations that are not present in (2), we nevertheless reach analogous conclusions on the resulting mixed-mode dynamics. Our study hence underpins the claim made in [14], namely, that Eq. (2) truly represents a canonical form. (We remark that a reduction of the so-called Wilson–Calloway model for the dopaminergic neuron [23] to (2) can be found in the related article [15]; our analysis will be similar in spirit to theirs.)

Finally, we note that the extended Bonhoeffer–van der Pol oscillator has been considered as a three time-scale system before, in [21], albeit in a slightly different formulation. Based on detailed asymptotics—which, incidentally, bears some resemblance to our approach—and numerical simulation, the author of that article was led to conclude the likely absence of stable periodic orbits of mixed-mode type in the system. Applying geometric singular perturbation theory, we disprove that conjecture rigorously.

This article is organised as follows. In Sect. 2, we study Eq. (1) in the standard two time-scale form of geometric singular perturbation theory, with one fast variable x and two slow variables (y, z) . In Sect. 2.1, we describe the singular flow that is obtained for $\varepsilon = 0$ in (1). Then, in Sect. 2.2, we locate so-called ‘folded equilibria,’ which are crucial to the generation of canard-induced SAOs in the observed mixed-mode time series, and we identify a ‘folded saddle-node of type II’ (FSN II) [13, 19] as the ‘organising centre’ for the dynamics. In Sect. 2.3, we introduce a local formulation for Eq. (1) close to that folded equilibrium; moreover, we define the bifurcation parameter μ —a combination of k_1 and B_0 —which unfolds the mixed-mode dynamics of (1). Finally, in Sect. 2.4, we apply standard geometric theory [6, 10] to approximate the global return mechanism which resets the flow to the SAO

regime after passage through the fold region, and which hence accounts for the LAO portion of the resulting mixed-mode time series.

In Sect. 3, we perform a proper three-scale analysis of the transformed ‘localised’ version of (1) obtained in Sect. 2, under the additional assumption that $k_3 = \mathcal{O}(\varepsilon)$. (For simplicity, and in agreement with the parameter regime considered in [17], we will assume $k_3 = 0.1 = \varepsilon$.) In Sect. 3.1, we study the local dynamics near the folded saddle-node identified in Sect. 2.2 by means of a ‘blow-up’ transformation [5, 12] which uncovers the near-integrable structure of the equations, thus desingularising the flow there. Next, we describe the entry into, and the exit from, the fold region, which completes our analysis of the local dynamics. In Sect. 3.2, we then combine the resulting asymptotic estimates with our description of the global return, thus obtaining an approximation for the first-return map of the three time-scale Bonhoeffer–van der Pol oscillator. In Sect. 3.3, we discuss the bifurcation structure of that map, with a particular focus on secondary (‘bifurcating’) canards and sectors of rotation; then, in Sect. 3.4, we outline a reduction to an essentially one-dimensional map, which we analyse in accordance with [14, 15].

Finally, in Sect. 4, we discuss our findings, and we illustrate them numerically; moreover, we present potential pointers for future research.

2 Two Time-Scale Analysis

Assuming, for the time being, that the parameter k_3 in Eq. (1c) does not scale with ε , we may interpret the equations in (1) as a fast-slow system in standard form that evolves on two distinct time-scales, the ratio of which is given by the singular perturbation parameter ε .

2.1 Reduced Flow

Setting $\varepsilon = 0$ in (1) and considering the resulting reduced equations, we find the (two-dimensional) critical manifold

$$\mathcal{S}_0 := \{(x, y, z) \mid y = \varphi(x, z) = -x(1 - x^2) - z, (x, y, z) \in \mathcal{D} \subset \mathbb{R}^3\},$$

where $\mathcal{D} := [-x_0, x_0] \times [-y_0, y_0] \times [-z_0, z_0]$ is a compact subset of \mathbb{R}^3 with $z_0 > \frac{\sqrt{3}}{9}$, $y_0 > \frac{2\sqrt{3}}{9} + z_0$, and $x_0 > \frac{2\sqrt{3}}{3}$; the corresponding layer dynamics is given by horizontal fibres in the x -direction, with y and z fixed. Solving $\frac{\partial \varphi}{\partial x}(x, z) = -(1 - 3x^2) = 0$ for x , one then readily verifies that \mathcal{S}_0 is normally hyperbolic except at the two fold lines $\ell^\pm := \{(x, y, z) \mid x = \pm \frac{\sqrt{3}}{3}, y = -z \mp \frac{2\sqrt{3}}{9}, z \in [-z_0, z_0]\}$, with z_0 as above. Hence, it follows that the manifold \mathcal{S}_0 can be written as the union of three sheets, $\mathcal{S}_0 = \mathcal{S}_0^{a-} \cup \mathcal{S}_0^r \cup \mathcal{S}_0^{a+}$, with $\mathcal{S}_0^{a\pm}$ attracting and \mathcal{S}_0^r repelling; here, \mathcal{S}_0^{a-} , \mathcal{S}_0^r , and \mathcal{S}_0^{a+} are defined by $x < -\frac{\sqrt{3}}{3}$, $x \in (-\frac{\sqrt{3}}{3}, \frac{\sqrt{3}}{3})$, and $x > \frac{\sqrt{3}}{3}$, respectively, with y and z varying accordingly. (An illustration of the resulting geometry—albeit in a transformed coordinate frame, to be introduced in Sect. 2.3 below—can be found in Fig. 1; here, we remark that the assumptions on x_0 , y_0 , and z_0 in the definition of the set \mathcal{D} above are made precisely to encapsulate that geometry.) For $\varepsilon > 0$ sufficiently small, we then denote the corresponding sheets of the slow manifold \mathcal{S}_ε by $\mathcal{S}_\varepsilon^{a-}$, $\mathcal{S}_\varepsilon^r$, and $\mathcal{S}_\varepsilon^{a+}$, respectively.

Next, we recall that we have opted to consider only the regime where $B_0 > 0$ in (1); then, it is easy to verify that the ‘left’ fold line ℓ^- is always of jump type in that regime, with a slow flow that is pointed in the direction of increasing y . As is well known, geometric singular

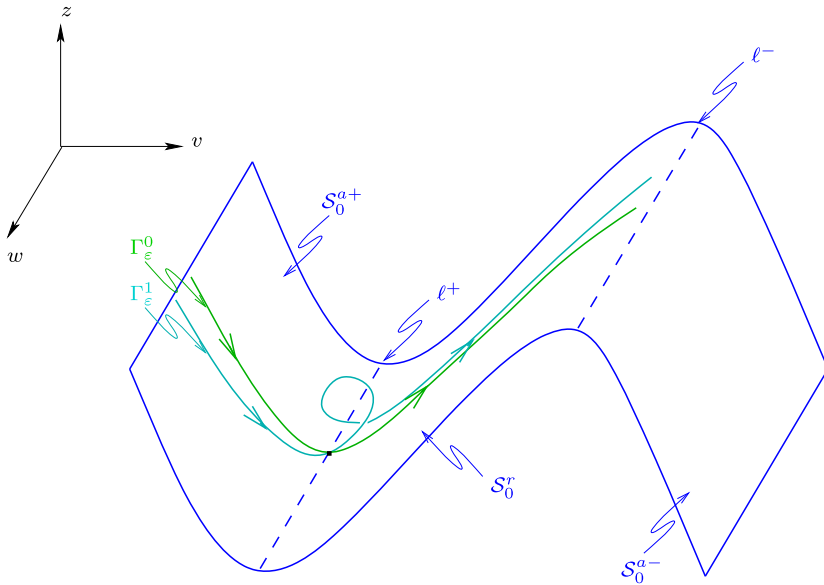


Fig. 1 Geometry of Eq. (6)

perturbation theory [6, 10] can be combined with the desingularisation technique known as ‘blow-up’ [4, 12] to describe the flow near l^- ; see also [20], where the resulting relaxation dynamics is studied from a geometric point of view.

The flow near the ‘right’ fold l^+ , on the other hand, is more involved; in particular, we argue that the presence of a (singular) Hopf bifurcation [8] near l^+ for $B_0 \approx \frac{1}{2}$ suggests the occurrence of complicated canard-type dynamics there, i.e., the existence of solutions that cross from the attracting sheet S_ε^{a+} to the repelling sheet S_ε^r , staying near the latter for extended periods of time before being repelled away. To describe the corresponding dynamics, we first verify the presence of ‘folded equilibria’ [19, 22] in (1), which are a necessary prerequisite for the existence of canard trajectories.

2.2 Folded Equilibria

To determine the folded equilibria of Eq. (1), we proceed as in [15, Sect. 2.4]: we set $\varepsilon = 0$ in (1a) and then differentiate the relation $\varphi(x, z) - y = 0$ with respect to time τ , obtaining $\dot{y} = \frac{\partial \varphi}{\partial x} \dot{x} + \frac{\partial \varphi}{\partial z} \dot{z} = -(1 - 3x^2)\dot{x} - \dot{z}$. Substituting for \dot{y} and \dot{z} from (1b) and (1c), respectively, we have

$$-(1 - 3x^2)\dot{x} = -x + k_1[x(1 - x^2) + z] + B_0 + k_3(-x - k_1z + B_0).$$

Appending Eq. (1c) and desingularising the resulting system by multiplication of the right-hand sides with a factor of $\frac{\partial \varphi}{\partial x}$, we find the projection of the reduced flow on S_0 onto the (x, z) -plane in a neighbourhood of l^+ :

$$\dot{x} = -x + k_1[x(1 - x^2) + z] + B_0 - k_3(x + k_1z - B_0), \tag{3a}$$

$$\dot{z} = k_3(x + k_1z - B_0)(1 - 3x^2). \tag{3b}$$

Now, ‘folded equilibria’ of Eq. (1) [15] correspond to equilibrium points (x_+, z_+) of (3) that satisfy $\frac{\partial \varphi}{\partial x}(x_+, z_+) = 0$, and that are hence located at

$$x_+ = \frac{\sqrt{3}}{3} \quad \text{and} \quad z_+ = \frac{3\sqrt{3}(1 - \sqrt{3}B_0)(1 + k_3) - 2\sqrt{3}k_1}{9k_1(1 - k_3)}. \tag{4}$$

(‘Regular’ equilibria of (3), i.e., equilibria that do not lie on ℓ^+ , are found by requiring that $x + k_1z - B_0 = 0$ and $-x + k_1[x(1 - x^2) + z] + B_0 = 0$ hold simultaneously.) For future reference, we note that z_+ depends on the parameters k_1, k_3 , and—most importantly— B_0 . Since, moreover, $\frac{\partial \varphi}{\partial x} < 0$ for $-\frac{\sqrt{3}}{3} < x < \frac{\sqrt{3}}{3}$, the desingularisation leading to (3) effectively reverses the direction of the flow on S_0^r , allowing for the existence of canard trajectories that can pass from S_0^{a+} to S_0^r via the folded equilibrium at $P^+ = (x_+, z_+)$; see again [19, 22] for details.

We claim that the point P^+ undergoes a saddle-node bifurcation on the fold line ℓ^+ for some critical value B_0^* of the parameter B_0 :

Lemma 1 *The folded equilibrium $P^+ = (x_+, z_+)$, with x_+ and z_+ defined as in Eq. (4), undergoes a saddle-node bifurcation of type II as B_0 passes through $B_0^* \equiv \frac{\sqrt{3}}{9}(3 - k_1)$.*

Proof Linearising Eq. (3) about P^+ , we obtain

$$J = \begin{bmatrix} -(1 + k_3) & k_1(1 - k_3) \\ -4\sqrt{3}k_3 \frac{3\sqrt{3} - \sqrt{3}k_1 - 9B_0}{9(1 - k_3)} & 0 \end{bmatrix}$$

for the Jacobian of the reduced flow at (x_+, z_+) , as given in (4). Since the trace of J is $-(1 + k_3)$, while the determinant is of the order k_3 , we deduce that one of the eigenvalues of J equals $-1 + \mathcal{O}(k_3)$, while the other is $\mathcal{O}(k_3)$. Solving $\det J = 0$ for B_0 , we find that the latter eigenvalue equals zero for $3 - k_1 - 3\sqrt{3}B_0 = 0$, which yields $B_0 = \frac{\sqrt{3}}{9}(3 - k_1) \equiv B_0^*$, as claimed.

Finally, it is straightforward to verify that the eigendirection corresponding to the zero eigenvalue for $B_0 = B_0^*$ is transverse to the fold line ℓ^+ , i.e., that P^+ is a *folded saddle-node of type II*; see [19] for details. (In fact, one calculates that the eigenvalue-eigenvector pairs of J for $B_0 = B_0^*$ are given by $\{-(1 + k_3), (1, 0)\}$ and $\{0, (k_1 \frac{1 - k_3}{1 + k_3}, 1)\}$, respectively.) \square

Remark 1 Alternatively, one can determine B_0^* by considering the $(2, 1)$ -entry of the Jacobian J : B_0^* is precisely the value of B_0 for which that entry equals zero. \square

In sum, one hence obtains the following picture for the projected reduced flow of Eq. (1): when $B_0 > B_0^*$, a stable node equilibrium exists on the ‘right’ (attracting) sheet S_0^{a+} of S_0 , while P^+ is a folded saddle; for $B_0 = B_0^*$, that equilibrium coalesces with P^+ in a transcritical bifurcation of a saddle and a node, i.e., the point P^+ undergoes a saddle-node bifurcation on the fold ℓ^+ . (In fact, one can show that P^+ is both a regular and a folded equilibrium in that case.) Finally, when $B_0 < B_0^*$ —which is the regime we are interested in— P^+ is a folded node, while a saddle equilibrium is found on the ‘middle’ (repelling) sheet S_0^r of S_0 .

2.3 Local Formulation

In this subsection, we rewrite Eq. (1) in a form that is more suitable for the following analysis; to that end, we perform a series of coordinate changes which transform (1) into an equivalent

set of equations that is centred on the ‘right’ fold line ℓ^+ . We begin by translating the folded equilibrium at P^+ to the origin by introducing the new variables

$$v = -(x - x_+), \quad p = y + z - (y_+ + z_+) = y + z + \frac{2}{9}\sqrt{3}, \quad \text{and} \quad q = z - z_+;$$

here, x_+ and z_+ are defined as in Eq. (4), while the constant in the definition of p is obtained by solving $0 = x_+(1 - x_+^2) + y_+ + z_+$, as found from (1a), for $y_+ + z_+$. (The change of sign in the definition of v additionally reflects the critical manifold \mathcal{S}_0 about the q -axis, thus bringing it into a more familiar configuration; clearly, that reflection reverses the location of the two sheets $\mathcal{S}_\varepsilon^{a\pm}$, with $\mathcal{S}_\varepsilon^{a+}$ becoming the ‘left’ attracting sheet and $\mathcal{S}_\varepsilon^{a-}$ the ‘right’ one.)

The system of equations resulting from the above transformation is given by

$$\varepsilon \dot{v} = \sqrt{3}v^2 - v^3 - p, \tag{5a}$$

$$\dot{p} = (1 + k_3)v + k_1(1 - k_3)q - k_1p, \tag{5b}$$

$$\dot{q} = k_3(v - k_1q - \mu), \tag{5c}$$

where $\mu = \frac{2}{1-k_3}(B_0^* - B_0)$ denotes a new parameter, with B_0^* defined as in the statement of Lemma 1.

Finally, to reduce these equations to a form that is as close as possible to the canonical system in (2), we rescale q by introducing the new variable $w = -k_1q$, and we abuse notation slightly, relabelling p as z for consistency with [14]:

$$\varepsilon \dot{v} = \sqrt{3}v^2 - v^3 - z, \tag{6a}$$

$$\dot{z} = (1 + k_3)v - (1 - k_3)w - k_1z, \tag{6b}$$

$$\dot{w} = k_1k_3(\mu - w - v). \tag{6c}$$

For future reference, we remark that the critical manifold \mathcal{S}_0 is given by $z = f(v) := \sqrt{3}v^2 - v^3$ in the context of Eq. (6); the corresponding reduced geometry of (1) in the singular limit of $\varepsilon = 0$ is sketched in Fig. 1.

2.4 Global Return Mechanism

Before considering in detail the local dynamics of (6) in a neighbourhood of the fold line ℓ^+ , we discuss the global return mechanism which reinjects the flow into the fold region after relaxation has occurred. As in [14, Sect. 2.1], we first define two sections, a section $\Sigma^{\text{in}} : \{v = -\rho\}$ through the attracting sheet \mathcal{S}_0^{a+} and a section $\Sigma^{\text{out}} : \{v = \delta\}$ across the fast foliation of \mathcal{S}_0 , with $\rho, \delta > 0$ small, but fixed, and $|z|$ and $|w|$ bounded; see Fig. 2 for an illustration. The global return from Σ^{out} to Σ^{in} under the flow of (6) can then be approximated to leading order via the slow evolution of v along the attracting sheets \mathcal{S}_0^{a-} and \mathcal{S}_0^{a+} of the critical manifold \mathcal{S}_0 , as illustrated in Fig. 3; in particular, one may neglect the transition from ℓ^+ to \mathcal{S}_0^{a-} and from ℓ^- to \mathcal{S}_0^{a+} , respectively, under the corresponding layer flow, as was also done in [14, Sect. 2.5].

Thus, we have the following result on the leading-order asymptotics of the map $\Pi^{\text{ret}} : \Sigma^{\text{out}} \rightarrow \Sigma^{\text{in}}$, the proof of which closely follows [14, Sect. 2.5] and [15, Sect. 3.3]:

Lemma 2 *Let $w_0 > 0$ be sufficiently small; then, the w -component of the global return map $\Pi^{\text{ret}} : \Sigma^{\text{out}} \rightarrow \Sigma^{\text{in}}$ satisfies*

$$\hat{w} := \Pi^{\text{ret}}(w) = w + k_1k_3 \left[3 \left(1 - \frac{1}{2}k_1 \right) \mu - \frac{1}{2}\sqrt{3}k_1 \right] \tag{7}$$

to leading order in k_3 and ε , for any $w \in [-w_0, w_0] \subset \Sigma^{\text{out}}$.

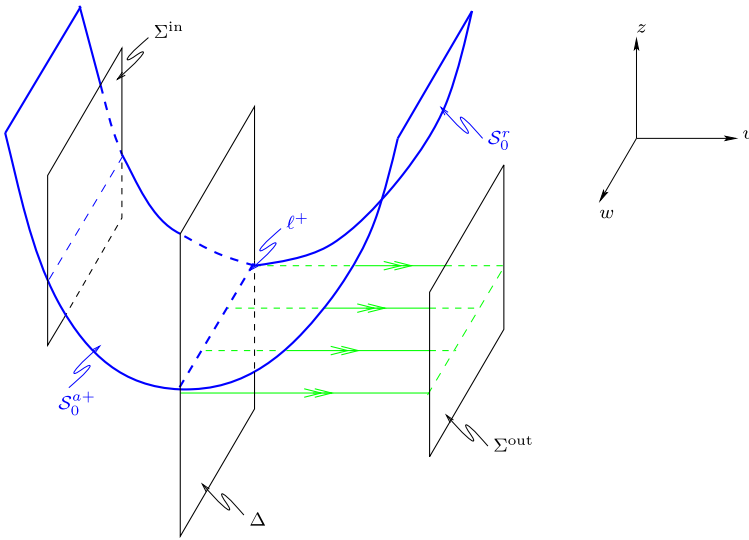


Fig. 2 Sections for the flow of (6)

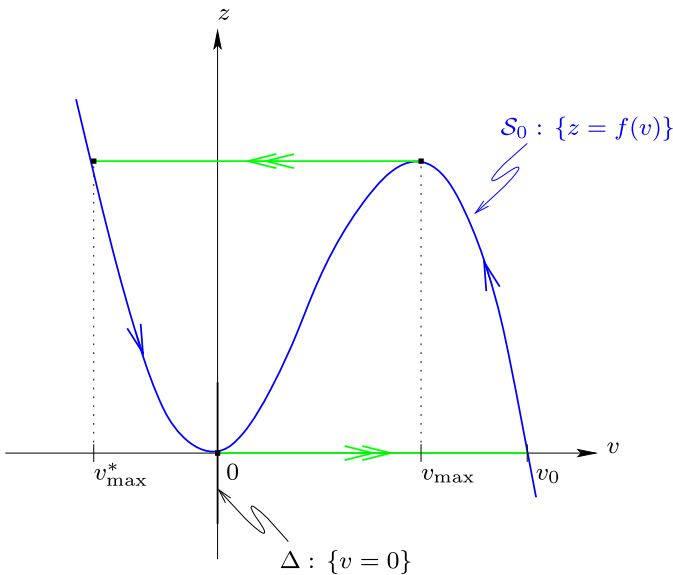


Fig. 3 Geometry of global return

Proof We consider the projection of the reduced flow corresponding to Eq. (6) onto the critical manifold S_0 , the accuracy of which will be sufficient for deriving the leading-order approximation for Π^{ret} considered here; cf. also [14, Sect. 2.5]. Proceeding as in Sect. 2.2, i.e., noting that $z = f(v)$ implies $\dot{z} = f'(v)\dot{v}$ and desingularising the resulting (v, w) -system by multiplication with a factor of $-f'(v)$, which is positive on the two attracting sheets $S_0^{a\pm}$ of S_0 , we find

$$\dot{v} = -(1 + k_3)v + (1 - k_3)w + k_1 f(v), \tag{8a}$$

$$\dot{w} = -k_1 k_3 f'(v)(\mu - v - w). \tag{8b}$$

Next, we note that $w = \mathcal{O}(1)$ in the parameter regime which is of interest to us, as $0 \lesssim k_3 \ll 1$ then, whereas $v = \mathcal{O}(1)$ and $z = \mathcal{O}(1)$ during the global return phase. (Specifically, numerical evidence suggests that one may assume $w = \mathcal{O}(k_3)$ throughout; see also Assumption 1 below.) Hence, approximating (8a) by $\dot{v} \approx -v + k_1 f(v)$ and neglecting the w -dependence in (8b), we obtain

$$\frac{dw}{dv} = k_1 k_3 \frac{f'(v)(\mu - v)}{v - k_1 f(v)}, \tag{9}$$

to lowest order in k_3 and ε . Now, we observe that, with k_1 fixed, the condition $|k_1 \frac{f(v)}{v}| < 1$ is certainly satisfied for v in some appropriately chosen (compact) interval. (In fact, for $k_1 = 0.35$, as in [17], it suffices to take $v \in [v_{\max}^*, v_0]$, where v_{\max}^* and v_0 are defined below, as $|\frac{f(v)}{v}| \leq \frac{4}{3}$ on that interval.) Hence, we may approximate $\frac{1}{v - k_1 f(v)} \approx \frac{1}{v} [1 + k_1 \frac{f(v)}{v}]$, which implies

$$\frac{dw}{dv} = k_1 k_3 \frac{f'(v)}{v} (\mu - v) \left[1 + k_1 \frac{f(v)}{v} \right]. \tag{10}$$

Finally, following [14, 15], we define

$$\mathcal{G}(v^*, v, \mu) := k_1 \int_{v^*}^v \frac{f'(\sigma)}{\sigma} (\mu - \sigma) \left[1 + k_1 \frac{f(\sigma)}{\sigma} \right] d\sigma;$$

then, we may write the leading-order solution to (10) as $\hat{w} = w + k_3 [\mathcal{G}(v_0, v_{\max}, \mu) + \mathcal{G}(v_{\max}^*, -\rho, \mu)]$, where the limits of integration are defined as $v_{\max} = \frac{2}{3}\sqrt{3}$, $v_{\max}^* = -\frac{1}{3}\sqrt{3}$, and $v_0 = \sqrt{3}$, with ρ as in the definition of the section Σ^{in} above. (Here, we have adopted the notation of [14], where v_{\max} is the value of v for which f attains its local maximum, $v_{\max}^* < 0$ is defined by the requirement that $f(v_{\max}^*) = f(v_{\max})$, and $v_0 > 0$ is the second, non-trivial zero of f ; cf. again Fig. 3.) Replacing $\mathcal{G}(v_{\max}^*, -\rho, \mu)$ with $\mathcal{G}(v_{\max}^*, 0, \mu)$, as was done in [14, Sect. 2.5], and evaluating the resulting integrals, we find (7), as claimed, which completes the proof. \square

Remark 2 While Π^{ret} is a function of the two variables z and w , it reduces to a one-dimensional map (in w) to the order considered here, by Eq. (7). Hence, we have opted to suppress the z -dependence of Π^{ret} in our notation. \square

In particular, given Lemma 2, we may approximate the critical value μ^c of μ beyond which the flow of (6) exhibits pure relaxation oscillation: requiring that $\hat{w} = w$ in (7), as in [14, Sect. 2.5], i.e., solving the term in square brackets therein for μ , we have

Corollary 1 *The critical μ -value μ^c for which mixed-mode dynamics ceases to exist in Eq. (6) is given by $\mu^c = \frac{1}{3} \frac{\sqrt{3}k_1}{2 - k_1}$, to lowest order in k_3 and ε .*

Evaluating μ for $k_1 = 0.35$, as in [17], we obtain $\mu^c = 0.070\sqrt{3} \approx 0.12247$, which is in good agreement with numerical simulation; see Sect. 4 below. (In fact, explicit integration of (9), and evaluation at the same limits as in the proof of Lemma 2, yields $\mu^c \approx 0.09769$, which is well within $\mathcal{O}(k_3^2, k_3\varepsilon)$ of the estimate given in Corollary 1, as expected.)

Remark 3 For future reference, we note that Eq. (7) yields an approximation for Π^{ret} which is accurate up to an $\mathcal{O}(\varepsilon^2 \ln \varepsilon)$ -error when $k_3 = \varepsilon$, as is assumed in the following section. In fact, projecting the flow of (6) onto the slow manifold \mathcal{S}_ε instead of onto \mathcal{S}_0 , one can show that the error incurred by Eqs. (8) and (9) is of the order $\mathcal{O}(\varepsilon^2)$ when $w = \mathcal{O}(\varepsilon)$, while an $\mathcal{O}(\varepsilon^2 \ln \varepsilon)$ -contribution is introduced through passage past the fold line ℓ^- ; see [20, Theorem 1] for details. \square

3 Three Time-Scale Analysis

Given the parameter regime studied by Sekikawa et al. [17], with $k_1 = 0.35$ and $\varepsilon = 0.1$, it seems reasonable to set $k_3 = \varepsilon$ in Eq. (6); then, the variable w will vary on a third (‘super-slow’) time scale, as (6c) implies $\dot{w} = \mathcal{O}(\varepsilon)$ throughout. (Since, clearly, $v = \mathcal{O}(1)$ and $z = \mathcal{O}(1)$ during relaxation, cf. the proof of Lemma 2 as well as Fig. 3, it follows that the variables v and z will remain ‘fast’ and ‘slow,’ respectively.)

Hence, replacing k_3 with ε and writing κ instead of k_1 for compactness, we obtain the system of equations

$$\varepsilon \dot{v} = \sqrt{3}v^2 - v^3 - z, \tag{11a}$$

$$\dot{z} = v - w - \kappa z + \varepsilon(v + w), \tag{11b}$$

$$\dot{w} = \varepsilon \kappa (\mu - w - v) \tag{11c}$$

from (6) which, together with the corresponding fast system

$$v' = \sqrt{3}v^2 - v^3 - z, \tag{12a}$$

$$z' = \varepsilon[v - w - \kappa z + \varepsilon(v + w)], \tag{12b}$$

$$w' = \varepsilon^2 \kappa (\mu - w - v), \tag{12c}$$

will be the starting point for our study of the three time-scale Bonhoeffer–van der Pol oscillator. (Here, the prime denotes differentiation with respect to the fast time $t = \frac{\tau}{\varepsilon}$.)

In the remainder of this article, we will characterise the mixed-mode dynamics that is induced by the flow of Eq. (11); as we will show below, the resulting asymptotics will be very similar ‘qualitatively’ to the picture painted in [14], even if some of the specifics of the analysis will differ. Following [14, 15], we will restrict the parameter μ —which we have identified as the relevant bifurcation parameter above—to some interval $(\underline{\mu}, \bar{\mu})$ on which stable ‘mixed’ MMO dynamics can unfold in (11). Since we will not consider the ‘pure’ relaxation (LAO) regime in (11), where $\mu > \mu^c$, we must have $\bar{\mu} \lesssim \mu^c$. However, we will also disregard the purely oscillatory (SAO) regime that is obtained for μ close to zero: as numerical simulation implies the occurrence of a (singular) Hopf bifurcation [8] $\mathcal{O}(\varepsilon)$ -close to the fold at ℓ^+ —and, hence, the onset of small-amplitude oscillatory dynamics—for $\mu \equiv \mu^H \approx 0.02072$, it follows that $\underline{\mu} \gtrsim \mu^H$ must hold; see Sect. 4 below for details.

It remains to show that the interval $(\underline{\mu}, \bar{\mu})$ is non-empty: since $\mu^c = \mathcal{O}(\varepsilon)$ in the parameter regime considered here, as stated in Sect. 2.4 above, while $\mu^H = \mathcal{O}(\varepsilon^2)$, we may conclude that the width of $(\underline{\mu}, \bar{\mu})$ is of the order $\mathcal{O}(\varepsilon^\alpha)$ for some $1 < \alpha < 2$ and, hence, that non-trivial mixed-mode dynamics will be observed in (11) as μ is varied in that interval; cf. also the discussion towards the end of [14, Sect. 2.2].

3.1 Local Dynamics

In this subsection, we consider Eq. (11) locally, in a neighbourhood of ℓ^+ . To that end, we first analyse the dynamics of (11)—or, equivalently, of (12)—in the fold region itself, by introducing an appropriate rescaling of the variables (v, z, w) near ℓ^+ ; then, we study the mechanisms which govern the entry of the flow into that region and the exit from it, respectively.

3.1.1 Fold Region

To describe the dynamics of Eq. (12) in a neighbourhood of the fold line ℓ^+ , we rescale the vector field there by writing

$$v = \sqrt{\varepsilon}\bar{v}, \quad z = \varepsilon\bar{z}, \quad w = \sqrt{\varepsilon}\bar{w}, \quad \text{and} \quad \bar{t} = \sqrt{\varepsilon}t. \tag{13}$$

Substituting into (12) and simplifying, we obtain the desingularised system of equations

$$\bar{v}' = \sqrt{3}\bar{v}^2 - \bar{z} - \sqrt{\varepsilon}\bar{v}^3, \tag{14a}$$

$$\bar{z}' = \bar{v} - \bar{w} - \kappa\sqrt{\varepsilon}\bar{z} + \varepsilon(\bar{v} + \bar{w}), \tag{14b}$$

$$\bar{w}' = \varepsilon\kappa[\mu - \sqrt{\varepsilon}(\bar{w} + \bar{v})]; \tag{14c}$$

as pointed out in [14], in the context of Eq. (2), the scale separation between v and z has been eliminated by the rescaling in (13). (Here, the prime now denotes differentiation with respect to the new time \bar{t} ; however, for simplicity of notation, we will frequently omit the bar in the following, writing again t instead.)

Based on numerical evidence (data not shown), we expect that $w = \mathcal{O}(\varepsilon)$ in Eq. (12), uniformly in t ; see also the proof of Lemma 2 above. Correspondingly, we will henceforth make the following assumption on $\bar{w} = \frac{w}{\sqrt{\varepsilon}}$, which may be verified *a posteriori* for the parameter regime considered here; details can be found in [14, Sect. 2.2].

Assumption 1 Let $\varepsilon \in [0, \varepsilon_0]$, with $\varepsilon_0 > 0$ sufficiently small; then, $\bar{w} = \mathcal{O}(\sqrt{\varepsilon})$ as $\varepsilon \rightarrow 0^+$ in (14), uniformly in \bar{t} .

In the singular limit, i.e., for $\varepsilon = 0$, Eq. (14) reduces to the planar system

$$\begin{aligned} \bar{v}' &= \sqrt{3}\bar{v}^2 - \bar{z}, \\ \bar{z}' &= \bar{v} - \bar{w}, \end{aligned} \tag{15}$$

in which \bar{w} is a (constant) parameter. The resulting flow is well-understood, as it underlies the study of classical two-dimensional canard explosion [5,12]. In particular, Eq. (15) is integrable for $\bar{w} = 0$, with a constant of motion of the form

$$H(\bar{v}, \bar{z}) = \frac{1}{2}e^{-2\sqrt{3}\bar{z}} \left(-\bar{v}^2 + \frac{\sqrt{3}}{3}\bar{z} + \frac{1}{6} \right); \tag{16}$$

see also [14, Eq. (2.5)]. Thus, level curves for (15) are defined by $H(\bar{v}, \bar{z}) = h$, with h real; the singular solution corresponding to $h = 0$, which is given by

$$\bar{v}_0^0(t) = (\bar{v}_0^0, \bar{z}_0^0)(t) = \left(\frac{\sqrt{3}}{6}t, \frac{\sqrt{3}}{12}t^2 - \frac{\sqrt{3}}{6} \right), \tag{17}$$

cf. [14, Eq. (2.6)], separates the closed level curves of H that are obtained for $h > 0$ from the open ones, which are characterised by $h < 0$. (Clearly, the former yield periodic solutions

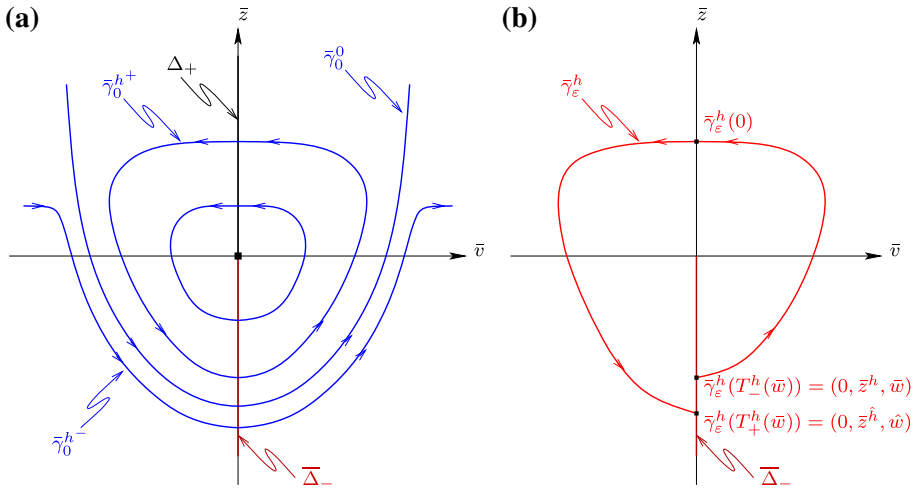


Fig. 4 Dynamics of Eq. (14). **a** $\varepsilon = 0$, **b** $\varepsilon > 0$

to Eq. (15), while the latter correspond to trajectories that leave the fold region; see [14] for details.) The geometry of (14) in the singular limit is illustrated in Fig. 4(a).

As in [14, Sect. 2.2], we introduce the following notation: we write Δ for the plane $v = 0$, with (z, w) in some compact subset of \mathbb{R}^2 ; see again Fig. 2. Then, $\overline{\Delta}$ denotes that same plane in the rescaled coordinates defined in (13), while $\overline{\Delta}_-$ stands for the half-plane $\overline{\Delta} \cap \{\bar{z} < 0\}$.

Remark 4 Here and in the following, \square will denote any object in the original (v, z, w) -coordinates, while the equivalent ‘blown-up’ object in $(\bar{v}, \bar{z}, \bar{w})$ -space will be written as $\overline{\square}$.

In our analysis, we will sometimes parametrise trajectories of (15) by their unique h -value; thus, we will write \bar{z}^h for the corresponding (unique) value of \bar{z} in $\overline{\Delta}_-$. Moreover, denoting by $\bar{\gamma}_\varepsilon^h(t)$ the solution to (14) which contains the point $(0, \bar{z}^h, \bar{w})$, we will assume that the time parametrisation is such that $\bar{\gamma}_\varepsilon^h(0)$ lies in $\overline{\Delta}_+ = \overline{\Delta} \setminus \overline{\Delta}_-$, as shown in Fig. 4(b). Let $T_\pm^h(\bar{w})$ denote the times for which $\bar{\gamma}_\varepsilon^h(T_\pm^h(\bar{w})) \in \overline{\Delta}_-$, where we note that, clearly, $T_-^h(\bar{w}) < 0 < T_+^h(\bar{w})$; see again Fig. 4(b). Then, we write $T^h(\bar{w}) := T_+^h(\bar{w}) - T_-^h(\bar{w})$ for the return time to $\overline{\Delta}_-$ under the flow of Eq. (14); for brevity, we define $T^h := T_+^h(0)$. Finally, one can show as in [14, Lemma A.2] that

$$T^h = \sqrt{-2 \ln h} + \mathcal{O}(1); \tag{18}$$

the above estimate will prove useful, since it implies $T^h = \mathcal{O}(\sqrt{-\ln \varepsilon})$ whenever $h = \mathcal{O}(\varepsilon^M)$ for some $M > 0$, as will be the case throughout the remainder of this section.

An approximation for the transition map $\overline{\Pi} : \overline{\Delta}_- \rightarrow \overline{\Delta}_-$, which describes the dynamics of (14) in the small-amplitude regime, can then be obtained in analogy to [14, Proposition 2.2]; we merely outline the derivation here, focussing on points at which the corresponding proof requires modification:

Proposition 1 *Let $\varepsilon \in [0, \varepsilon_0]$, with $\varepsilon_0 > 0$ sufficiently small, and suppose that $h = \mathcal{O}(\varepsilon^M)$ for some $M > 0$. Then, the transition map $\overline{\Pi} : \overline{\Delta}_- \rightarrow \overline{\Delta}_-$ for (14) is of the form*

$$(\hat{h}, \hat{w}) := \overline{\Pi}(h, \bar{w}) = (h + \sqrt{\varepsilon} d_{\sqrt{\varepsilon}}^h + \bar{w} d_{\bar{w}}^h + \mathcal{O}[(\sqrt{\varepsilon} + \bar{w})^2], \bar{w} + \varepsilon \kappa \mu T^h(\bar{w}) + \mathcal{O}(\varepsilon \sqrt{\varepsilon})), \tag{19}$$

where

$$d_{\sqrt{\varepsilon}}^h = \int_{-T^h}^{T^h} \nabla H(\bar{\gamma}_0^h(t)) \cdot (-\bar{v}_0^h(t)^3, -\kappa \bar{z}_0^h(t))^T dt \tag{20}$$

and

$$d_{\bar{w}}^h = \int_{-T^h}^{T^h} \nabla H(\bar{\gamma}_0^h(t)) \cdot (0, -1)^T dt. \tag{21}$$

Proof The expression for the h -component of $\bar{\Pi}$ is obtained via an adaptation of the argument in [14, Sect. 2.2]: due to the presence of an additional term of the order $\mathcal{O}(\sqrt{\varepsilon}z)$, Eq. (14b) is not in the form of the extended system formulated in [14, Eq. (2.8)]. However, denoting by \hat{h} the image of h under $\bar{\Pi}$, we still have

$$\begin{aligned} \hat{h} - h &= H(0, \bar{z}^{\hat{h}}) - H(0, \bar{z}^h) = \int_{T_-^h(\bar{w})}^{T_+^h(\bar{w})} \frac{d}{dt} H(\bar{\gamma}_\varepsilon^h(t)) dt \\ &\sim \int_{T_-^h(\bar{w})}^{T_+^h(\bar{w})} \nabla H(\bar{\gamma}_0^h(t)) \cdot (\bar{v}', \bar{z}')^T \Big|_{\bar{\gamma}_0^h(t)} dt = \sqrt{\varepsilon} d_{\sqrt{\varepsilon}}^h + \bar{w} d_{\bar{w}}^h; \end{aligned}$$

thus, the only difference to the proof of [14, Proposition 2.2] lies in the definition of the coefficient $d_{\sqrt{\varepsilon}}^h$ in (20), as was also the case in the corresponding Eq. (45a) of [15]. (In fact, a straightforward calculation shows that the contribution from the \bar{z} -dependent term in (14b) to that coefficient is non-zero.)

Similarly, the derivation of the \bar{w} -component of $\bar{\Pi}$ has to be adapted slightly, as we cannot simply integrate Eq. (14c). Instead, we express \bar{v} from (14b) and substitute into (14c), obtaining

$$\bar{w}' = -2\kappa\varepsilon\sqrt{\varepsilon}\bar{w} + \varepsilon\kappa[\mu - \sqrt{\varepsilon}\bar{z}'(t)] + \mathcal{O}(\varepsilon^2). \tag{22}$$

The solution of the corresponding homogeneous equation is given by $\bar{w}_h = C e^{-2\kappa\varepsilon\sqrt{\varepsilon}t}$. By variation of constants, we find $C'(t) = \varepsilon\kappa(\mu - \sqrt{\varepsilon}\bar{z}')e^{2\kappa\varepsilon\sqrt{\varepsilon}t}$ and, hence,

$$C(t) = \frac{\mu}{2\sqrt{\varepsilon}} (e^{2\kappa\varepsilon\sqrt{\varepsilon}t} - e^{2\kappa\varepsilon\sqrt{\varepsilon}T_-^h(\bar{w})}) - \kappa\varepsilon\sqrt{\varepsilon} \int_{T_-^h(\bar{w})}^t \bar{z}'(s)e^{2\kappa\varepsilon\sqrt{\varepsilon}s} ds$$

after integration. (Here, $T_-^h(\bar{w})$ is defined as above; in particular, we cannot simply translate the initial time to zero, as Eq. (22) is non-autonomous.) The full solution to (22) can then be expressed as

$$\begin{aligned} \bar{w}(t) &= C e^{-2\kappa\varepsilon\sqrt{\varepsilon}t} + \frac{\mu}{2\sqrt{\varepsilon}} (1 - e^{-2\kappa\varepsilon\sqrt{\varepsilon}[t-T_-^h(\bar{w})]}) \\ &\quad - \kappa\varepsilon\sqrt{\varepsilon} \int_{T_-^h(\bar{w})}^t \bar{z}'(s)e^{2\kappa\varepsilon\sqrt{\varepsilon}s} ds \cdot e^{-2\kappa\varepsilon\sqrt{\varepsilon}t}. \end{aligned} \tag{23}$$

Writing \bar{w} for the initial value of $\bar{w}(t)$ to determine $C = \bar{w}e^{2\kappa\varepsilon\sqrt{\varepsilon}T_-^h(\bar{w})}$ in (23), evaluating the resulting expression at $T_+^h(\bar{w})$ —i.e., after the return to $\bar{\Delta}_-$ has been completed—and expanding the exponential term via $e^{-2\kappa\varepsilon\sqrt{\varepsilon}t} = 1 - 2\kappa\varepsilon\sqrt{\varepsilon}t + \mathcal{O}(\varepsilon^3t^2)$, we find

$$\begin{aligned} \hat{w} &= \bar{w}[1 - 2\kappa\varepsilon\sqrt{\varepsilon}T^h(\bar{w})] + \varepsilon\kappa\mu T^h(\bar{w}) - \kappa\varepsilon\sqrt{\varepsilon} \int_{T_-^h(\bar{w})}^{T_+^h(\bar{w})} \bar{z}'(t)e^{2\kappa\varepsilon\sqrt{\varepsilon}t} dt \cdot e^{-2\kappa\varepsilon\sqrt{\varepsilon}T_+^h(\bar{w})} \\ &\quad + \mathcal{O}(\varepsilon^2). \end{aligned} \tag{24}$$

(Here, we recall that $T^h(\bar{w}) = T_+^h(\bar{w}) - T_-^h(\bar{w})$ denotes the return time to $\bar{\Delta}_-$, as before.) Since $\bar{w} = \mathcal{O}(\sqrt{\varepsilon})$, and since we may assume $T^h(\bar{w}) = \mathcal{O}(\sqrt{-\ln \varepsilon})$, see also Eq. (18), we can neglect the $2\kappa\varepsilon\sqrt{\varepsilon}\bar{w}T^h(\bar{w})$ -term in (24). Hence, it remains to estimate the integral term therein: integrating by parts, we obtain

$$\begin{aligned} &\int_{T_-^h(\bar{w})}^{T_+^h(\bar{w})} \bar{z}'(t)e^{2\kappa\varepsilon\sqrt{\varepsilon}t} dt \cdot e^{-2\kappa\varepsilon\sqrt{\varepsilon}T_+^h(\bar{w})} \\ &= \bar{z}(t)e^{2\kappa\varepsilon\sqrt{\varepsilon}t} \Big|_{T_-^h(\bar{w})}^{T_+^h(\bar{w})} \cdot e^{-2\kappa\varepsilon\sqrt{\varepsilon}T_+^h(\bar{w})} - 2\kappa\varepsilon\sqrt{\varepsilon} \int_{T_-^h(\bar{w})}^{T_+^h(\bar{w})} \bar{z}(t)e^{2\kappa\varepsilon\sqrt{\varepsilon}t} dt \cdot e^{-2\kappa\varepsilon\sqrt{\varepsilon}T_+^h(\bar{w})}. \end{aligned}$$

Now, taking into account that $\bar{z} = \mathcal{O}(1)$ in the fold region, as well as that the exponential factor multiplying the second (integral) term on the right-hand side is bounded by one, the contribution from the latter is clearly of higher order; the first (boundary) term gives

$$\begin{aligned} \bar{z}(t)e^{2\kappa\varepsilon\sqrt{\varepsilon}t} \Big|_{T_-^h(\bar{w})}^{T_+^h(\bar{w})} \cdot e^{-2\kappa\varepsilon\sqrt{\varepsilon}T_+^h(\bar{w})} &= \left[\bar{z}(T_+^h(\bar{w}))e^{2\kappa\varepsilon\sqrt{\varepsilon}T_+^h(\bar{w})} - \bar{z}(T_-^h(\bar{w}))e^{2\kappa\varepsilon\sqrt{\varepsilon}T_-^h(\bar{w})} \right] \\ &\quad \times e^{-2\kappa\varepsilon\sqrt{\varepsilon}T_+^h(\bar{w})} \\ &= \bar{z}(T_+^h(\bar{w})) - \bar{z}(T_-^h(\bar{w})) + \mathcal{O}(\varepsilon\sqrt{\varepsilon}T_{\pm}^h(\bar{w})) \end{aligned}$$

to leading order, since any exponential factors that occur can again be approximated by $1 + \mathcal{O}(\varepsilon\sqrt{\varepsilon}T_{\pm}^h(\bar{w}))$, and since $\bar{z}(T_{\pm}^h(\bar{w})) = \mathcal{O}(1)$. Finally, we claim that $\bar{z}(T_+^h(\bar{w})) - \bar{z}(T_-^h(\bar{w})) = \mathcal{O}(\sqrt{\varepsilon})$, which is easily verified by considering the constant of motion H , as defined in Eq. (16): assuming that $H(0, \bar{z}(T_+^h(\bar{w}))) - H(0, \bar{z}(T_-^h(\bar{w}))) = \mathcal{O}(\sqrt{\varepsilon})$ in $\bar{\Delta}_-$, one can solve perturbatively for $\bar{z}(T_+^h(\bar{w}))$ in terms of $\bar{z}(T_-^h(\bar{w}))$. (Alternatively, one may resort to the well-known asymptotics of the Lambert W function [16, Sect. 1.5].)

In sum, it follows that the integral term in (24) is of the order $\mathcal{O}(\varepsilon^2)$, which implies $\hat{w} = \bar{w} + \varepsilon\kappa\mu T^h(\bar{w}) + \mathcal{O}(\varepsilon\sqrt{\varepsilon})$, as claimed, completing the proof. \square

3.1.2 Entry Mechanism

Next, we consider the entry of the flow induced by Eq. (12) into the fold region; in other words, we will approximate the transition between the sections Σ^{in} and $\bar{\Delta}_-$, as defined in Sects. 2.4 and 3.1.1, respectively. Following [14, Sect. 2.3], we introduce an ‘intermediate’ section $\bar{\Delta}^{\text{in}} : \{\bar{v} = -\alpha\}$ (in rescaled coordinates), with $0 < \alpha < \rho$ small and fixed. Correspondingly, in the proof of Proposition 2 below, we first study the transition between Σ^{in} and Δ^{in} , followed by that between $\bar{\Delta}^{\text{in}}$ and $\bar{\Delta}_-$:

Proposition 2 *Let $(z^{\text{in}}, w^{\text{in}}) \in \Sigma^{\text{in}}$; then, for $\varepsilon \in [0, \varepsilon_0]$ sufficiently small, the transition map $\Pi^{\text{in}} : \Sigma^{\text{in}} \rightarrow \bar{\Delta}_-$ satisfies*

$$\begin{aligned} (h^-, \bar{w}^-) &:= \Pi^{\text{in}}(z^{\text{in}}, w^{\text{in}}) \\ &= \left(\sqrt{\varepsilon} d_{\sqrt{\varepsilon}}^- + \frac{w^{\text{in}}}{\sqrt{\varepsilon}} d_{\bar{w}}^- + \mathcal{O}[(\sqrt{\varepsilon} + \bar{w})^2], \frac{w^{\text{in}}}{\sqrt{\varepsilon}} + w^{\text{in}} \sqrt{3\kappa\mu} \sqrt{\varepsilon} \ln \varepsilon + \mathcal{O}(\sqrt{\varepsilon}) \right), \end{aligned} \tag{25}$$

where

$$\begin{aligned} d_{\sqrt{\varepsilon}}^- &= \int_{-\infty}^0 \nabla H(\bar{\gamma}_0^0(t)) \cdot (-\bar{v}_0^0(t)^3, -\kappa \bar{z}_0^0(t))^T dt \quad \text{and} \\ d_{\bar{w}}^- &= \int_{-\infty}^0 \nabla H(\bar{\gamma}_0^0(t)) \cdot (0, -1)^T dt. \end{aligned}$$

Proof As in the proof of [14, Proposition 2.3], we consider a projectivisation of the flow of (11); however, due to the z -dependence of Eq. (11b), we cannot *a priori* discount the $\mathcal{O}(\varepsilon)$ -correction to the reduced flow on S_0^{a+} in our case. Hence, we write $z = z(v, w, \varepsilon) = Z_0(v) + \varepsilon Z_1(v, w) + \mathcal{O}(\varepsilon^2)$, where $Z_0(v) = -v^3 + \sqrt{3}v^2 = f(v)$. Substituting the above Ansatz into (11b), noting that $\dot{z} = \frac{\partial Z_0}{\partial v} \dot{v} + \varepsilon \left(\frac{\partial Z_1}{\partial v} \dot{v} + \frac{\partial Z_1}{\partial w} \dot{w} \right) + \mathcal{O}(\varepsilon^2)$, and making use of Eq. (11a), we find

$$Z_1(v, w) = -\frac{v - w - \kappa f(v)}{f'(v)} = -\frac{v - w - \kappa(\sqrt{3}v^2 - v^3)}{2\sqrt{3}v - 3v^2}.$$

Since, moreover, $\dot{z} = \left(\frac{\partial Z_0}{\partial v} + \varepsilon \frac{\partial Z_1}{\partial v} \right) \dot{v} + \mathcal{O}(\varepsilon\sqrt{\varepsilon})$, as $\frac{\partial Z_1}{\partial v} = \mathcal{O}(1)$ and $\frac{\partial Z_1}{\partial w} = \mathcal{O}(\varepsilon^{-\frac{1}{2}})$ for $v \in [-\rho, -\alpha\sqrt{\varepsilon}]$ and $w = \mathcal{O}(\varepsilon)$, while $\dot{w} = \mathcal{O}(\varepsilon)$ due to Eq. (11c), a straightforward calculation yields the following projection of (11a) onto the slow manifold S_ε^{a+} :

$$\begin{aligned} [2\sqrt{3}v - 3v^2 + \mathcal{O}(\varepsilon)]\dot{v} &= v - w - \kappa \left[\sqrt{3}v^2 - v^3 - \varepsilon \frac{v - w - \kappa(\sqrt{3}v^2 - v^3)}{2\sqrt{3}v - 3v^2} \right] \\ &\quad + \varepsilon(v + w) + \mathcal{O}(\varepsilon\sqrt{\varepsilon}). \end{aligned}$$

The corresponding projected system on S_ε^{a+} that is obtained from (11) is then given by

$$\dot{v} = - \left\{ v - w - \kappa \left[\sqrt{3}v^2 - v^3 - \varepsilon \frac{v - w - \kappa(\sqrt{3}v^2 - v^3)}{2\sqrt{3}v - 3v^2} \right] + \varepsilon(v + w) \right\}, \tag{26a}$$

$$\dot{w} = -\varepsilon\kappa(\mu - w - v)(2\sqrt{3}v - 3v^2) \tag{26b}$$

after desingularisation, i.e., multiplication with a factor of $-\frac{\partial z}{\partial v} = -[2\sqrt{3}v - 3v^2 + \mathcal{O}(\varepsilon)]$, which is certainly positive for ε sufficiently small and $v \leq -\alpha\sqrt{\varepsilon}$, as above. (Here, we have neglected the resulting $\mathcal{O}(\varepsilon^2)$ -correction in (26b), as well as terms of order $\mathcal{O}(\varepsilon\sqrt{\varepsilon})$ and upwards in (26a), as both are irrelevant to the order considered here.)

Next, we define the new (projective) variable $W = \frac{w}{v}$, and we rewrite Eq. (26) in terms of W to obtain

$$\dot{v} = -v\mathcal{F}(v, W, \kappa, \varepsilon), \tag{27a}$$

$$\dot{W} = W\mathcal{F}(v, W, \kappa, \varepsilon) - \varepsilon\kappa(\mu - vW - v)[2\sqrt{3} - 3v + \mathcal{O}(\sqrt{\varepsilon})]. \tag{27b}$$

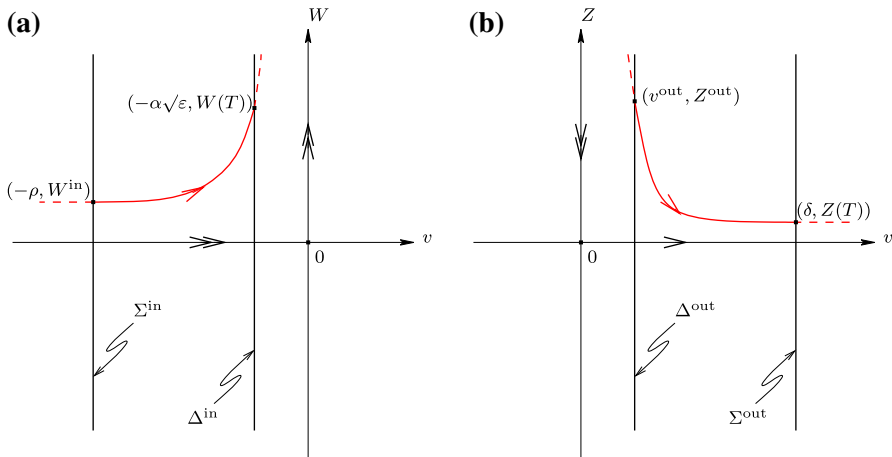


Fig. 5 Illustration of entry and exit mechanisms. **a** Geometry of Eq. (28), **b** geometry of Eq. (31)

Since the function \mathcal{F} , which is defined as

$$\mathcal{F}(v, W, \kappa, \varepsilon) = 1 - W - \kappa \left[\sqrt{3}v - v^2 - \varepsilon \frac{1 - W - \kappa(\sqrt{3}v - v^2)}{2\sqrt{3}v - 3v^2} \right] + \varepsilon(1 + W),$$

is non-zero—and, in fact, positive—for $(v, W, \kappa, \varepsilon)$ sufficiently small, we may perform a transformation of time in Eq. (27) to cancel a factor of \mathcal{F} from the right-hand sides therein. (Without loss of generality, and with an abuse of notation, we again denote the new rescaled time by τ .) Next, we expand the resulting equations, taking into account that

$$Z_1(v, W) \equiv Z_1(v, vW) = \frac{1}{2v} \left[\frac{\sqrt{3}}{3} - \left(\kappa - \frac{1}{2} \right) v + \mathcal{O}(v^2) \right],$$

to leading order in W , and noting that $W = \mathcal{O}(\sqrt{\varepsilon})$ due to $v \in [-\rho, -\alpha\sqrt{\varepsilon}]$ and $w = \mathcal{O}(\varepsilon)$. Neglecting terms of second order and upwards in (v, W) , we thus have the following approximation for (27), which is analogous to [14, Eq. (2.25)]:

$$\dot{v} = -v, \tag{28a}$$

$$\dot{W} = (1 - 2\sqrt{3}\kappa\mu\varepsilon)W - 2\sqrt{3}\kappa\mu\varepsilon + (3\mu + 2\sqrt{3} - 6\kappa\mu)\kappa\varepsilon v. \tag{28b}$$

Since Eq. (28a) can be integrated explicitly, with $v(\tau) = -\rho e^{-\tau}$, we may substitute into (28b) and solve for $W(\tau)$; given the (rescaled) transition time $T = \ln \frac{\rho}{\alpha\sqrt{\varepsilon}}$ between Σ^{in} and Δ^{in} , we then evaluate the resulting solution to obtain

$$W(T) = \frac{\rho}{\alpha\sqrt{\varepsilon}} W^{\text{in}} (1 + \sqrt{3}\kappa\mu\varepsilon \ln \varepsilon) + \mathcal{O}(\sqrt{\varepsilon}),$$

as sketched in Fig. 5(a). Finally, we make use of the fact that $w(T) = -\alpha\sqrt{\varepsilon}W(T)$, as well as of $w^{\text{in}} = -\rho W^{\text{in}}$, to find $w(T) = w^{\text{in}}(1 + \sqrt{3}\kappa\mu\varepsilon \ln \varepsilon) + \mathcal{O}(\varepsilon)$.

It remains to consider the transition from $\bar{\Delta}^{\text{in}}$ to $\bar{\Delta}_-$; in analogy to [14], we denote the corresponding map by $\bar{\Pi}^{\text{in}}$. To that end, we recall the proof of Proposition 1 from the previous subsection, taking into account that we need to transform between original and

rescaled (‘blown-up’) coordinates; cf. Eq. (13). Then, it is easy to see that

$$(h^-, \bar{w}^-) = \bar{\Pi}(\bar{z}, \bar{w}) = (\sqrt{\varepsilon}d_{\sqrt{\varepsilon}}^- + \bar{w}d_{\bar{w}}^- + \mathcal{O}[(\sqrt{\varepsilon} + \bar{w})^2], \bar{w} + 2\sqrt{3}\alpha\kappa\mu\varepsilon + \mathcal{O}(\varepsilon^2)), \tag{29}$$

where $d_{\sqrt{\varepsilon}}^-$ and $d_{\bar{w}}^-$ are defined as in the statement of the proposition; see also [14, Eq. (2.30)]. (In particular, one observes that these coefficients correspond to the solution curve $\bar{\gamma}_0^0$ defined in Eq. (17), as well as that the transition time between $\bar{\Delta}^{\text{in}}$ and $\bar{\Delta}_-$ is given by $\bar{T}^{\text{in}} = 2\sqrt{3}\alpha$, as in [14].)

Finally, we combine the estimate for \bar{w}^- in (29) with the asymptotics of $w(T)$ derived above, noting that the condition for $(\bar{v}, \bar{z}, \bar{w})$ to lie on a trajectory originating in $\mathcal{S}_\varepsilon^{a+}$ is, in fact, expressed by the h^- -component of $\bar{\Pi}(\bar{z}, \bar{w})$. Taking into account that $\bar{w} = \frac{w}{\sqrt{\varepsilon}}$, we obtain Eq. (25), as claimed. □

We remark that the term $\frac{w^{\text{in}}}{\sqrt{\varepsilon}}$ in (25) remains bounded as $\varepsilon \rightarrow 0^+$, since $w^{\text{in}} = \mathcal{O}(\varepsilon)$ by Assumption 1; hence, $(h^-, \bar{w}^-) \rightarrow (0, 0)$ in that limit, which is consistent with the definition of the singular solution $\bar{\gamma}_0^0$.

Remark 5 It follows from the first part of the proof of Proposition 2 that the flow between Σ^{in} and Δ^{in} can, in fact, be approximated by the reduced dynamics on the critical manifold \mathcal{S}_0^{a+} , as was also done in [14, Proposition 2.3]. (Specifically, our expression for $w(T)$ agrees with the one obtained there, i.e., the $\mathcal{O}(\varepsilon)$ -correction due to Z_1 turns out to be irrelevant *a posteriori*.) Similarly, the second part of that proof implies that our approximation of the transition between $\bar{\Delta}^{\text{in}}$ and $\bar{\Delta}_-$ via the singular (integrable) system in (15) is sufficiently accurate, as the resulting \bar{T}^{in} -dependent correction to \bar{w}^- does not even enter Eq. (25) to the order considered here.

3.1.3 Exit Mechanism

As in the previous subsection, the analysis of the exit from the fold region is divided into two portions: first, we consider the transition between the section $\bar{\Delta}_-$ and its image under the flow of (14) at time $T^{h,\text{out}}(\bar{w}) := -T^{-h}(\bar{w})$, which we denote by $\bar{\Delta}^{\text{out}}$; then, we study the transition from $\bar{\Delta}^{\text{out}}$ to the section Σ^{out} defined in Sect. 2.4. (Naturally, we are interested in $h < 0$ here, since trajectories with $h > 0$ cannot leave the fold region, as noted in Sect. 3.1.1.)

We require the following notation: we write C_ε^a and C_ε^r for the intersection curves of $\mathcal{S}_\varepsilon^{a+}$ and $\mathcal{S}_\varepsilon^r$ with the Poincaré section Δ that was defined in Sect. 3.1.1. (Here, we remark that these curves were denoted by C_ε^{\pm} in [14]; however, due to the fact that the canard phenomenon is observed at ℓ^+ instead of at ℓ^- in our case, recall Sect. 2, we had to adapt our notation accordingly.) Finally, as in [14, Sect. 2.4], we introduce a change of variable in \bar{z} such that the curve C_ε^r becomes parallel to the \bar{w} -axis in $\bar{\Delta}$ when written in terms of the new variable \bar{z} :

Proposition 3 *Let $(h, \bar{w}) \in \bar{\Delta}_-$, with $h < 0$ and $h = \mathcal{O}(\varepsilon^M)$ for some $M > 0$, and let $\varepsilon \in [0, \varepsilon_0]$ be sufficiently small. Then, the transition map $\Pi^{\text{out}} : \bar{\Delta}_- \rightarrow \Sigma^{\text{out}}$ is of the form*

$$(z^{\text{out}}, w^{\text{out}}) := \Pi^{\text{out}}(h, \bar{w}) = (\varepsilon\bar{z}^{\text{out}} + \mathcal{O}(\varepsilon \ln \varepsilon), \sqrt{\varepsilon}\bar{w} + \varepsilon\sqrt{\varepsilon}\kappa\mu T^{h,\text{out}}(\bar{w}) + \mathcal{O}(\varepsilon\sqrt{\varepsilon})), \tag{30}$$

where \tilde{z}^{out} is the \tilde{z} -value corresponding to $h^{\text{out}} = h + \sqrt{\varepsilon}d_{\sqrt{\varepsilon}}^{\text{out}} + \bar{w}d_{\bar{w}}^{\text{out}}$, with

$$d_{\sqrt{\varepsilon}}^{\text{out}} = - \int_0^{T^{h,\text{out}}(\bar{w})} \nabla H(\tilde{\gamma}_0^h(t)) \cdot (-\tilde{v}_0^h(t)^3, -\kappa \tilde{z}_0^h(t))^T dt \quad \text{and}$$

$$d_{\bar{w}}^{\text{out}} = - \int_0^{T^{h,\text{out}}(\bar{w})} \nabla H(\tilde{\gamma}_0^h(t)) \cdot (0, -1)^T dt.$$

Proof As the proof is very similar to that of [14, Proposition 2.4], we merely sketch it here, emphasising the requisite modifications.

Let $(h, \bar{w}) \in \bar{\Delta}_-$, and let $\bar{\Pi}^{\text{out}}$ denote the time- $T^{h,\text{out}}(\bar{w})$ transition map between $\bar{\Delta}_-$ and the (implicitly defined) section $\bar{\Delta}^{\text{out}} := \bar{\Pi}^{\text{out}}(\bar{\Delta}_-)$. Then, it follows immediately from the near-integrability of Eq. (14) that

$$(h^{\text{out}}, \bar{w}^{\text{out}}) := \bar{\Pi}^{\text{out}}(h, \bar{w}) = (h + \sqrt{\varepsilon}d_{\sqrt{\varepsilon}}^{\text{out}} + \bar{w}d_{\bar{w}}^{\text{out}} + \mathcal{O}[(\sqrt{\varepsilon} + \bar{w})^2], \bar{w} + \varepsilon\kappa\mu T^{h,\text{out}}(\bar{w}) + \mathcal{O}(\varepsilon\sqrt{\varepsilon})),$$

where $d_{\sqrt{\varepsilon}}^{\text{out}}$ and $d_{\bar{w}}^{\text{out}}$ are defined as in the statement of the proposition; see also the proof of Proposition 1.

The second part of the transition—from $\bar{\Delta}^{\text{out}}$ to Σ^{out} —is studied via a change of variables, with $z = v^2Z$, which can be considered as a ‘phase-directional’ chart in ‘blow-up’ phase space; see again [14] for details. Rewriting (12) in terms of (v, Z, w) and rescaling time by dividing out a (positive) factor of $\Phi(v, Z) = v^2(-Z + \sqrt{3} - v)$ from the right-hand sides of the resulting equations, we obtain

$$v' = 1, \tag{31a}$$

$$Z' = -2\frac{Z}{v} + \frac{\varepsilon}{v\Phi(v, Z)} \left[1 - \frac{w}{v} - \kappa vZ + \varepsilon \left(1 + \frac{w}{v} \right) \right], \tag{31b}$$

$$w' = \frac{\varepsilon^2}{\Phi(v, Z)} \kappa(\mu - w - v). \tag{31c}$$

(With an abuse of notation, the prime now denotes differentiation with respect to the new, rescaled time.) To leading order, Eqs. (31a) and (31b) are identical to [14, Eqs. (2.45a), (2.45b)]. Also, as there, $v^{\text{out}} = \mathcal{O}(\sqrt{\varepsilon}T^{h,\text{out}}) = \mathcal{O}(\sqrt{-\varepsilon \ln \varepsilon})$ and $w = \mathcal{O}(\varepsilon)$ imply $\frac{w}{v} = \mathcal{O}(\sqrt{\varepsilon})$ and $\frac{dw}{dt} = \mathcal{O}(\varepsilon(\ln \varepsilon)^{-1})$. Expanding Φ , we then find $Z' = -\frac{2}{v}Z + \frac{\varepsilon}{v^3}\frac{\sqrt{3}}{3}[1 - \kappa vZ + \mathcal{O}(v, Z)]$; moreover, as $vZ = \mathcal{O}(1)$, we obtain $z(T) = \varepsilon\tilde{z}^{\text{out}} + \mathcal{O}(\varepsilon \ln \varepsilon)$ for the corresponding leading-order solution, in analogy to [14]. (Here, T denotes the transition time from Δ^{out} to Σ^{out} , as illustrated in Fig 5b)

It remains to consider the evolution of w : to that end, we integrate Eq. (12c) directly. Expanding the solution and noting that $T \leq \frac{2\sqrt{3}}{3v^{\text{out}}} + \frac{1}{3} \ln \varepsilon + \mathcal{O}(1)$, again by [14], we deduce

$$w(T) = \sqrt{\varepsilon}\bar{w}^{\text{out}} + \varepsilon^2 \left(\kappa\mu T - \sqrt{\varepsilon}\kappa\bar{w}^{\text{out}}T + \int_{v^{\text{out}}}^{\delta} \frac{v}{\Phi(v,0)} dv \right) + \mathcal{O}(\varepsilon^3)$$

$$= \sqrt{\varepsilon}\bar{w} + \varepsilon\sqrt{\varepsilon}\kappa\mu T^{h,\text{out}}(\bar{w}) + \mathcal{O}(\varepsilon\sqrt{\varepsilon}).$$

(As in the proof of [14, Proposition 2.4], one easily sees that the integral term in the above expression is of higher order, by combining the fact that $\int \frac{v}{\Phi(v,0)} dv = -\frac{\sqrt{3}}{3} \ln \frac{v}{\sqrt{3+v}} + c$ with the asymptotics of v^{out} .) Finally, collecting the above estimates, we have Eq. (30), as claimed. \square

3.2 Return Map Π

In this subsection, we approximate the ‘composite’ return map Π that is induced by the flow of (11) in the three time-scale regime considered here: combining the asymptotic formulae for Π^{ret} , $\bar{\Pi}$, Π^{in} , and Π^{out} , as obtained in Lemma 2 and Propositions 1 through 3, respectively, we may write

$$\Pi(h, \bar{w}) = \begin{cases} \bar{\Pi}(h, \bar{w}) & \text{if } h > 0, \\ \Pi^{\text{in}} \circ \Pi^{\text{ret}} \circ \Pi^{\text{out}}(h, \bar{w}) & \text{if } h < 0; \end{cases} \tag{32}$$

for future reference, we note that Π is defined as a Poincaré map from Δ_- —or, rather, its ‘blown-up’ analogue $\bar{\Delta}_-$ —to itself.

Obviously, the definition of Π thus depends on the sign of h : for positive h , the point of intersection of the corresponding trajectory with Δ lies above C_ε^r , forcing the flow back into the fold region; for negative h , on the other hand, that point lies below C_ε^r , allowing the trajectory to leave and undergo relaxation. Correspondingly, in the resulting time series, one hence obtains an SAO in the former case and an LAO in the latter; since, moreover, the sign of h may change after each application of Π , iteration of the above procedure generates the mixed-mode patterns that are observed in Eq. (11). A cartoon illustration of how the segment 1^2 —in which two SAOs are followed by one LAO—is produced by iterating Π can be found in Fig. 6.

While the Poincaré map Π in (32) is a function of the two variables h and \bar{w} , a simplification can be achieved by eliminating the h -dependence of Π , as in [14, Sect. 3]. The derivation of the corresponding ‘partially reduced’ map, which is sufficiently accurate for our purposes, is outlined below.

In a first step, a union of curves C_ε^j is inductively defined as follows: we write $C_\varepsilon^j := \bar{\Pi}(\{(h, \bar{w}) \in C_\varepsilon^{j-1} \mid h > 0\})$, with $C_\varepsilon^0 \equiv C_\varepsilon^a$. (Hence, for $j \geq 1$, one may simply interpret C_ε^j as the image of C_ε^a under the j th iterate $\bar{\Pi}^j$ of $\bar{\Pi}$.) Then, it can be shown as in [14, Sect. 3.1] that the curve C_ε^j may be written as the graph of a function $h^j(\bar{w})$ which is ‘almost linear’ in \bar{w} , at least for $|\bar{w}|$ sufficiently small; the resulting geometry of these curves is summarised in Fig. 7. Finally, following [14, Proposition 3.1], it is possible to prove that there exists some positive integer k such that, for $1 \leq j \leq k$, Π^j will be exponentially close in ε to the union of the curves $\bigcup_{j=1}^k C_\varepsilon^j$; in other words, the restriction of Π to the set $\bigcup C_\varepsilon^j$ will incur (at most) an exponentially small error.

Gathering the results of Sects. 2.4 and 3.1.1 through 3.1.3 and assuming $(\bar{w}, h^j(\bar{w})) \in \bigcup C_\varepsilon^j$, we thus have the following approximation for the partially reduced map $\Pi(\bar{w}) \equiv \Pi(h^j(\bar{w}), \bar{w})$:

$$\Pi(\bar{w}) = \begin{cases} \bar{w} + \varepsilon \kappa \mu T^{h^j(\bar{w})}(\bar{w}) + \mathcal{O}(\varepsilon \sqrt{\varepsilon}) & \text{if } h^j(\bar{w}) > 0, \\ \bar{w} + \varepsilon \kappa \mu T^{h^j(\bar{w}), \text{out}}(\bar{w}) + \bar{w} \sqrt{3} \kappa \mu \varepsilon \ln \varepsilon \\ \quad + \sqrt{\varepsilon} \kappa [3(1 - \frac{1}{2} \kappa) \mu - \frac{1}{2} \sqrt{3} \kappa] + \mathcal{O}(\varepsilon) & \text{if } h^j(\bar{w}) < 0; \end{cases} \tag{33}$$

cf. also [14, Eq. (3.5)]. (Here, we have replaced k_3 with ε in Eq. (7), by assumption, and we have again written κ instead of k_1 ; moreover, we note that the error incurred by (7) is of

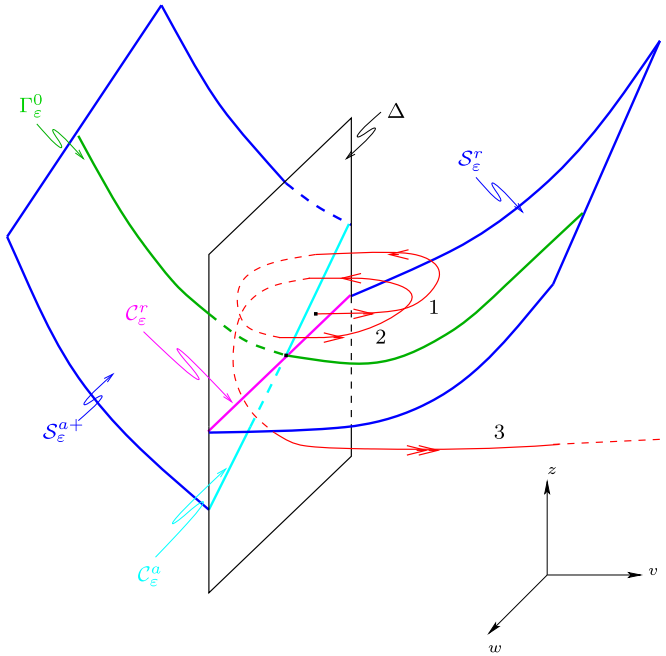
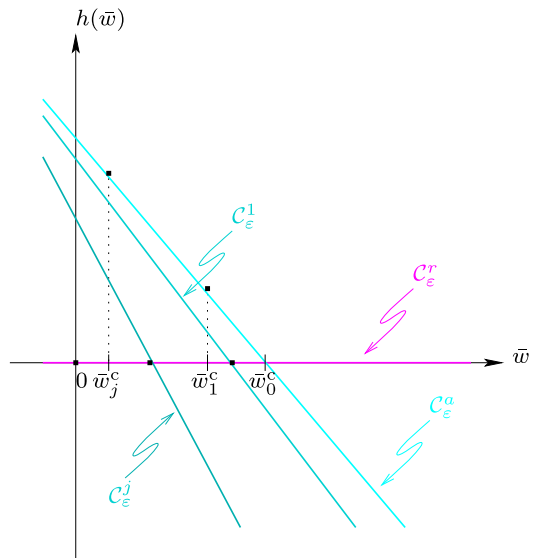


Fig. 6 Generation of mixed-mode dynamics by Π

Fig. 7 Curves C_ϵ^j for $j \geq 0$.



the order $\mathcal{O}(\epsilon)$, by Remark 3.) Since, trivially, none of the \bar{w} -independent terms in (33) will enter the derivative of Π with respect to \bar{w} , to be considered below, such terms will not be relevant for the following analysis.

3.2.1 Derivative of Π

Given Eq. (33), we immediately conclude that

$$\frac{d\Pi}{d\bar{w}} \sim \begin{cases} 1 + \varepsilon\kappa\mu \frac{dT^{h^j(\bar{w})}(\bar{w})}{d\bar{w}} & \text{if } h^j(\bar{w}) > 0, \\ 1 + \varepsilon\kappa\mu \frac{dT^{h^j(\bar{w}),\text{out}}(\bar{w})}{d\bar{w}} & \text{if } h^j(\bar{w}) < 0, \end{cases} \tag{34}$$

to leading order in ε . Estimates for the derivatives of the transition times $T^{h^j(\bar{w})}$ and $T^{h^j(\bar{w}),\text{out}}$ can be obtained verbatim as in [14, Sect. 3.2], as they are based on the asymptotics of the near-integrable system in (14). (Here, we recall that the only difference to the corresponding Eq. (2.3) in [14], to the order considered here, is due to the \bar{z} -dependence of (14b). Thus, the definition of the coefficient $d_{\sqrt{\varepsilon}}^h$ includes an additional contribution from \bar{z}_0^h in our case; cf. Eq. (20).) In sum, we thus find

$$\frac{dT^{h^j(\bar{w})}(\bar{w})}{d\bar{w}} \sim -\frac{2}{h^j(\bar{w})} \frac{1}{\sqrt{-2 \ln h^j(\bar{w})}} (j + 1) d_{\bar{w}}^0$$

and

$$\frac{dT^{h^j(\bar{w}),\text{out}}(\bar{w})}{d\bar{w}} \sim \frac{1}{h^j(\bar{w})} \frac{1}{\sqrt{-2 \ln h^j(\bar{w})}} (j + 1) d_{\bar{w}}^0.$$

3.3 Secondary Canards and Sectors of Rotation

Following [14, Sect. 1], we define the *strong canard* $\Gamma_\varepsilon (\equiv \Gamma_\varepsilon^0)$ as the trajectory of Eq. (12) which lies in the the transverse intersection of the attracting sheet $\mathcal{S}_\varepsilon^{a+}$ and the repelling sheet $\mathcal{S}_\varepsilon^r$ of the slow manifold \mathcal{S}_ε , for ε positive and sufficiently small. (As discussed in Sect. 3.1.1, Γ_ε is to lowest order described by the ‘special’ solution $\bar{\gamma}_0^0$ in the fold region, cf. (17), which organises the flow of the rescaled Eq. (14) in the singular limit.) Clearly, the strong canard corresponds to a ‘critical’ value \bar{w}_0^c of \bar{w} which equals, in fact, the \bar{w} -coordinate of the point of intersection of the curves C_ε^a and C_ε^r defined in Sect. 3.2; details can be found in [14, Sect. 1]. Similarly, for $j \geq 1$, we may define \bar{w}_j^c as the \bar{w} -coordinate of the point of intersection of C_ε^j with C_ε^r ; see again Fig. 7. The corresponding trajectory of (12) is called the *j*th *secondary canard* Γ_ε^j , and undergoes *j* SAOs (‘loops’) in the fold region before relaxation; recall Fig. 1, where the trajectories Γ_ε^j are sketched for $j = 0, 1$. Correspondingly, we call the \bar{w} -interval $(\bar{w}_j^c, \bar{w}_{j-1}^c)$ the *j*th sector of rotation, and we denote it by RS^j [14, Sect. 3.3].

To estimate \bar{w}_0^c to leading order in ε , we follow [14], demanding that $\hat{h} = h$; recall Proposition 1. Approximating $\pm T^h \sim \pm T^0 = \pm \infty$ in Eqs. (20) and (21) and evaluating ∇H at γ_0^0 , as defined in (17), we find $d_{\sqrt{\varepsilon}}^0 = \frac{1}{48}(1 + 2\kappa)\sqrt{2\pi}\varepsilon$ and $d_{\bar{w}}^0 = -\frac{1}{2\sqrt{3}}\sqrt{2\pi}\varepsilon$ —see also [14, Eq. (2.18)]—and, hence,

$$\bar{w}_0^c = -\frac{d_{\sqrt{\varepsilon}}^0}{d_{\bar{w}}^0} \sqrt{\varepsilon} + \mathcal{O}(\varepsilon) = \frac{\sqrt{3}}{24}(1 + 2\kappa)\sqrt{\varepsilon} + \mathcal{O}(\varepsilon). \tag{35}$$

Numerical simulation (data not shown) suggests excellent agreement with the above estimate for \bar{w}_0^c , even for the ‘large’ value of $\varepsilon = 0.1$ considered here. (Specifically, taking $\kappa = 0.35$, as before, we find $\bar{w}_0^c \sim \frac{2651}{68330}\sqrt{3} \approx 0.03880$.)

The other key quantity of interest, apart from the critical value \bar{w}_0^c of \bar{w} , concerns the width of the sectors of rotation RS^j , as defined above. To obtain the corresponding estimate,

we need to account for additional terms in the expansion for the transition map $\bar{\Pi}$ introduced in Sect. 3.1.1. (In fact, by combining the resulting two estimates, we may approximate the critical \bar{w} -values $\{\bar{w}_j^c\}$ for $j = 1, \dots, k$.)

Thus, we now consider the partially decoupled truncated system of equations

$$\bar{v}' = \sqrt{3}\bar{v}^2 - \bar{z} - \sqrt{\varepsilon}\bar{v}^3 + \sqrt{\varepsilon}F(0, 0) + \bar{w}G(0, 0), \tag{36a}$$

$$\bar{z}' = \bar{v} - \bar{w} - \kappa\sqrt{\varepsilon}\bar{z} + \varepsilon(\bar{v} + \bar{w}), \tag{36b}$$

$$\bar{w}' = \varepsilon\kappa\mu, \tag{36c}$$

which is defined in analogy to [14, Eq. (3.15)]. We note that Eq. (36) differs from the ‘rescaled’ system in (14) in two points: first, $\bar{w}(t)$ is not assumed to be constant; rather, Eq. (14c) is approximated by $\bar{w}' \sim \varepsilon\kappa\mu$, which yields $\bar{w}(t) \sim \bar{w} + \varepsilon\kappa\mu t$ after integration, where \bar{w} is some initial value. Second, the inclusion of higher-order terms in $\sqrt{\varepsilon}$ and \bar{w} in the \bar{v} -equation—which are multiplied by appropriately defined functions $F(\bar{w}, \sqrt{\varepsilon})$ and $G(\bar{w}, \sqrt{\varepsilon})$, respectively, that are, to leading order, evaluated at $(\bar{w}, \sqrt{\varepsilon}) = (0, 0)$ —is due to the transformation to the new variable \bar{z} ; see Sect. 3.1.3 and [14, Proposition 2.4] for details.

Finally, let $\bar{\Pi}_0$ denote the ‘reduced’ transition map for the system that is obtained by appending $\bar{w}' = 0$ to Eqs. (36a) and (36b). Then, one has the following result; cf. also [14, Proposition 3.2]:

Proposition 4 *Let $\bar{\Pi} : \bar{\Delta}_- \rightarrow \bar{\Delta}_-$ denote the return map for (14), and let $\varepsilon \in [0, \varepsilon_0]$ be sufficiently small. Then,*

$$\bar{\Pi}(h, \bar{w}) = \begin{pmatrix} P_h \bar{\Pi}_0(h, \bar{w}) + \varepsilon\kappa\mu\mathcal{K}(h) + \mathcal{O}(\varepsilon\sqrt{\varepsilon}) \\ \bar{w} + 2\varepsilon\kappa\mu T^h + \mathcal{O}(\varepsilon\sqrt{\varepsilon}) \end{pmatrix}, \tag{37}$$

where P_h is the projection onto the \bar{h} -coordinate, with $P_h \bar{\Pi}_0(h, \bar{w}) = \hat{h}$ as in Proposition 1, and

$$\mathcal{K}(h) = \int_{-T^h}^{T^h} \nabla H(\bar{\gamma}_0^h(t)) \cdot (G(0, 0), -1)^T (t + T^h) dt.$$

(In particular, one can show that $\mathcal{K}(h) = 2d_w^0 T^h + \mathcal{O}(1)$, where d_w^0 is defined as in Eq. (21); see [14, Lemma A.5].)

Proof As in the proof of [14, Proposition 3.2], one considers the partially decoupled truncated equations

$$\begin{aligned} \bar{v}' &= \sqrt{3}\bar{v}^2 - \bar{z} - \sqrt{\varepsilon}\bar{v}^3 + \sqrt{\varepsilon}F(0, 0) + (\bar{w} + \varepsilon\kappa\mu t)G(0, 0), \\ \bar{z}' &= \bar{v} - \bar{w} - \varepsilon\kappa\mu t - \kappa\sqrt{\varepsilon}\bar{z} + \varepsilon(\bar{v} + \bar{w} + \varepsilon\kappa\mu t). \end{aligned} \tag{38}$$

Since the above system agrees with [14, Eq. (3.17)] to leading order—apart from the additional $\kappa\sqrt{\varepsilon}\bar{z}$ -term, which, however, only affects the definition of $d_{\sqrt{\varepsilon}}^h$, as seen in the proof of Proposition 1—we find

$$P_h \bar{\Pi} \sim P_h \bar{\Pi}_0 + \varepsilon\kappa\mu\mathcal{K}(h) + \varepsilon \int_{-T^h}^{T^h} \nabla H(\bar{\gamma}_0^h(t)) \cdot (0, \bar{v}_0^h) dt.$$

Here, we have neglected terms of second order and upwards in (ε, \bar{w}) ; moreover, we note that any contribution coming from terms involving $F(0, 0)$ and $G(0, 0)$ evaluates to zero by

symmetry: as in the proof of [14, Proposition 2.2], we have $(\bar{v}_0^h, \bar{z}_0^h)(-t) = (-\bar{v}_0^h, \bar{z}_0^h)(t)$ on $\bar{\gamma}_0^h$. Finally, making again use of the oddness of \bar{v}_0^h , one can show that the integral term in the above expression vanishes. In sum, one hence obtains the refined expansion for $\bar{\Pi}$ in Eq. (37), as claimed, which completes the proof. \square

Given the result of Proposition 4, as well as Eq. (18), one can show as in [14, Proposition 3.3] that the width of the j th sector of rotation RS^j is approximately given by

$$\Delta \bar{w} := \bar{w}_j^c - \bar{w}_{j-1}^c \sim -2\varepsilon\kappa\mu\sqrt{-2 \ln \varepsilon}. \tag{39}$$

The above estimate is confirmed by numerical simulation (data not shown) and implies, in particular, that all sectors of rotation are of the same width to leading order for ε fixed, as well as that the sector RS^j is located ‘to the left’ of RS^{j-1} for any $j \geq 1$ due to $\Delta \bar{w} < 0$; see [14, Sect. 3.3] for details. (Undoing the rescaling in (13), one finds $\Delta w = \mathcal{O}(\varepsilon\sqrt{-\varepsilon \ln \varepsilon})$ for the corresponding estimate in terms of the original w -variable.) Consequently, it follows again as in [14, Sect. 3.3] that we will always observe a finite number of SAOs in any mixed-mode time series of (12); cf. also Sect. 4 below.

3.4 Reduced Return Map Φ

The final step in our analysis of the return map Π consists in a further reduction to a simplified, one-dimensional map $\Phi : \mathcal{C}_\varepsilon^a \rightarrow \mathcal{C}_\varepsilon^a$, which can be defined as follows [14, Sect. 3.4]: for $k \geq 0$,

$$\Phi(\bar{w}) = P_{\bar{w}}(\Pi^{\text{in}} \circ \Pi^{\text{ret}} \circ \Pi^{\text{out}} \circ \bar{\Pi}^k(h^0(\bar{w}), \bar{w})) \text{ if } (h^0(\bar{w}), \bar{w}) \in RS^k.$$

(Here, $P_{\bar{w}}$ denotes the projection onto the \bar{w} -coordinate, as before.) While the map Φ is hence defined on the single curve $\mathcal{C}_\varepsilon^a$ instead of on a union of curves $\bigcup \mathcal{C}_\varepsilon^j$, and while it is unimodal on each of the sectors of rotation RS^k , it has discontinuities at the boundaries between these sectors. The dynamics of Φ was studied in detail in Sect. 3.6 of [14]; here, we merely sketch the derivation of some of its properties that are relevant to us.

One such property concerns the derivative of Φ (with respect to \bar{w}) on RS^k ; the resulting estimate will allow us to characterise the contraction, or expansion, under Φ . Making use of the definition of Π^{in} , Π^{ret} , Π^{out} , and $\bar{\Pi}$, in combination with the Chain Rule and the fact that $h^j(\bar{w}^j) = \mathcal{O}(\varepsilon\sqrt{-\ln \varepsilon})$, we conclude as in [14, Lemma 3.5] that

$$\Phi'(\bar{w}) = 1 - \varepsilon\kappa\mu d_w^0 \frac{1}{\sqrt{-2 \ln \varepsilon}} \left(\sum_{j=0}^{k-1} \frac{2(j+1)}{h^j(\bar{w}^j)} + \frac{k+1}{h^k(\bar{w}^k)} \right) \sim 1 - \frac{\omega_k(\nu)}{4 \ln \varepsilon}; \tag{40}$$

see, in particular, [14, Eqs. (3.32), (3.33)]. Here, \bar{w}^j is the j th iterate of some initial \bar{w} -value \bar{w}^0 under $\bar{\Pi}$, and the auxiliary function ω_k is defined as

$$\omega_k(\nu) = \sum_{j=0}^{k-1} \frac{1}{k-j-\nu} - \frac{1}{2\nu},$$

where $\nu \in [0, 1]$ for $k \geq 1$, while $\nu > 0$ when $k = 0$.

Given the above estimate for Φ' , one can, for instance, show that the map Φ has a (local) minimum in each sector RS^k , i.e., at some \bar{w} -value \bar{w}_{min}^k . Moreover, one may write $\Phi(\bar{w}_{\text{min}}^k) = \Phi_{\text{min}} + \mathcal{O}(\varepsilon)$, with

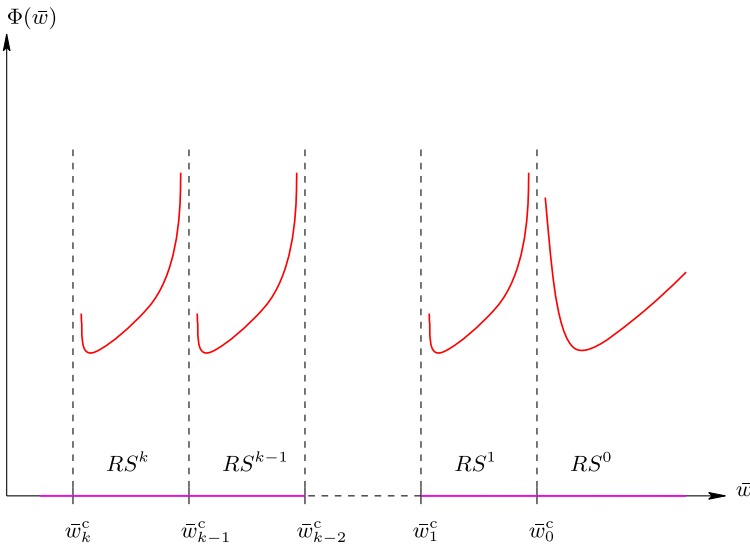


Fig. 8 Reduced return map Φ

$$\begin{aligned} \Phi_{\min} &\sim \bar{w}_0^c + \sqrt{\varepsilon} [\mathcal{G}(v_0, v_{\max}, \mu) + \mathcal{G}(v_{\max}^*, 0, \mu)] + \varepsilon \kappa \mu T^{h(\bar{w}_{\min}^0), \text{out}} \\ &\sim \sqrt{\varepsilon} \left[3\kappa \left(1 - \frac{1}{2}\kappa \right) \mu - \frac{1}{2} \sqrt{3} \left(\kappa^2 - \frac{1}{6}\kappa - \frac{1}{12} \right) \right] + \varepsilon \kappa \mu \sqrt{-2 \ln \varepsilon}; \end{aligned}$$

recall Eqs. (35), (7), (33), and (18), where the latter implies, in particular, $T^h \sim \sqrt{-2 \ln \varepsilon}$. Hence, it follows that Φ assumes the same minimum value (to leading order) for any $k = 0, 1, 2, \dots$; cf. [14, Eq. (3.36)]. A qualitative illustration of the map Φ is given in Fig. 8.

Next, we investigate the existence and stability of ‘regular’ mixed-mode periodic orbits with signature 1^k ; specifically, we estimate the width of the corresponding μ -interval $(\underline{\mu}^k, \bar{\mu}^k)$. In analogy to [14, Theorem 3.7], we obtain

Proposition 5 *Let $K > 0$ be arbitrary, but fixed; then, there is some (small) $\varepsilon_0 > 0$ such that, for $k = 1, \dots, K$ and $\varepsilon \in [0, \varepsilon_0]$, the periodic orbit of type 1^k exists and is stable when $\mu \in (\underline{\mu}^k, \bar{\mu}^k)$, with*

$$\Delta \mu^k := \bar{\mu}^k - \underline{\mu}^k \sim -\frac{\underline{\mu}^k \kappa}{\sqrt{2} D_\mu} \frac{\sqrt{\varepsilon}}{\sqrt{-\ln \varepsilon}} \int_{v_{-2}^k}^{v_0^k} \omega_k(v) dv. \tag{41}$$

Here, v_{-2}^k and v_0^k are defined by $\omega_k(v_{-2}^k) = 8 \ln \varepsilon$ and $\omega_k(v_0^k) = 0$, respectively, and

$$D_\mu = \frac{d}{d\mu} [\mathcal{G}(v_0, v_{\max}, \mu) + \mathcal{G}(v_{\max}^*, 0, \mu)]$$

is found by differentiating Eq. (7) with respect to μ .

Proof The proof of Eq. (41) is based on the observation that periodic orbits with signature 1^k correspond to fixed points of Φ , i.e., to solutions of $\Phi(\bar{w}, \mu) = \bar{w}$. The stability of those points follows from the second estimate for Φ' in Eq. (40), as one can show that $|\Phi'(\bar{w}, \mu)| < 1$ if

and only if $v \in (v_{-2}^k, v_0^k)$ in ω_k , with v_{-2}^k and v_0^k as defined above. Implicit differentiation then gives

$$\frac{d\mu}{d\bar{w}} = -\frac{\frac{\partial}{\partial \bar{w}} \Phi(\bar{w}, \mu) - 1}{\frac{\partial}{\partial \mu} \Phi(\bar{w}, \mu)} \sim \frac{1}{4 \ln \varepsilon} \frac{\omega_k(v)}{D_\mu \sqrt{\varepsilon}};$$

here, we have again used (40) as well as the estimate $\frac{\partial}{\partial \mu} \Phi(\bar{w}, \mu) \sim D_\mu \sqrt{\varepsilon}$.

Finally, applying the Fundamental Theorem of Calculus, we find

$$\Delta \mu^k = \int_{\bar{w}(\underline{\mu}^k)}^{\bar{w}(\bar{\mu}^k)} \frac{d\mu}{d\bar{w}} d\bar{w} \sim \frac{\Delta \bar{w}^k}{4 D_\mu \sqrt{\varepsilon} \ln \varepsilon} \int_{v_{-2}^k}^{v_0^k} \omega_k(v) dv.$$

Approximating $\Delta \bar{w}^k$ by $\Delta \bar{w} \sim -2\varepsilon \kappa \mu \sqrt{-2 \ln \varepsilon}$, recall Eq. (39), we obtain (41), as claimed. □

(The restriction to $k \leq K$ in the statement of Proposition 5 is due to the fact that our asymptotics is not uniform in k with respect to ε ; see [14, Proposition 3.4].) Since the remainder of the analysis presented in [14, Sect. 3.6] carries over *mutatis mutandis* to the context of Eq. (12), we do not retrace it here. Rather, we emphasise that the resulting mixed-mode dynamics, which will be discussed in detail in Sect. 4 below, is qualitatively equivalent to that of the canonical Eq. (2).

4 Discussion

In this article, we have studied mixed-mode oscillatory behaviour in a three-dimensional extended Bonhoeffer–van der Pol oscillator whose dynamics evolves on three distinct time-scales, thus complementing results previously obtained in [17]. To that end, we have transformed the governing equations into a form that is close to a simplified ‘prototypical’ model system which was proposed by Krupa et al. [14]; in the process, we have identified one bifurcation parameter that unfolds the mixed-mode dynamics generated by Eq. (1), expressing it as a function of two of the original parameters in the system. (An alternative approach, which was suggested recently (Kuehn C, 2013, Personal communication) and which we are currently considering, involves ‘mapping’ (1) onto a prototypical model proposed by Koper [11]; see also [3] for details.) We have sketched how the analysis of [14] can be adapted to the present context, which has allowed us to characterise the mixed-mode patterns that will ‘generically’ occur in (1), as well as to estimate the relevant parameter intervals. Recalling that the signature L^k encodes the segment consisting of k SAOs and L LAOs, and consulting Sect. 3.6 of [14], we may conclude that,

- (i) for $L = 1$, orbits contain segments of the form
 - (a) 1^k (possibly repeated some number of times),
 - (b) 1^{k-1} (possibly repeated some number of times), and
 - (c) 1^{k-2} , preceded by 1^k and followed by 1^{k-1} or 1^k ;
- (ii) for $L = 2$, only segments of the type 2^1 or 2^2 will occur;
- (iii) for $L \geq 2$, only segments of the form L^1 will be observed;

see Theorem 3.10, Proposition 3.11, and Corollary 3.12 of [14]. (For a detailed interpretation, and discussion, of the resulting mixed-mode dynamics, the reader is referred to [14, Sect. 4]

and [15, Sect. IV].) The above predictions are supported by numerical simulation, which was performed in MAPLE for the parameter regime considered by Sekikawa et al. [17]—with $\varepsilon = 0.1$, $k_1 = 0.35$, and B_0 close to $\frac{1}{2}$ in (1)—under the additional assumption that $k_3 = 0.1(=\varepsilon)$. (Specifically, we have simulated the corresponding transformed system of equations in (12) for values of μ close to μ^c , where we recall that $\kappa \equiv k_1$.) Throughout, we have set the initial condition to $(v, z, w)(0) = (0, 0, -0.01)$, unless explicitly stated otherwise; moreover, we have illustrated the resulting time series starting at time $t = 10^3$, after all transients have subsided.

As expected, we observe the unfolding of an entire family of non-trivial MMOs upon variation of the parameter μ : in Fig. 9(a), we still have relaxation, while (periodic) orbits with signature L^1 for $L = 6, 4, 3$, and 2—the latter two of which are separated by a ‘mixed’ pattern of the form $3^1 2^1$ —occur with decreasing μ , as shown in Fig. 9(b)–(f).

Then, as μ is decreased further, a transition is observed towards $L = 1$, beginning with the $2^1 1^1$ -type pattern displayed in Fig. 10(a). That pattern is followed by stable orbits of type $1^k, k = 1, 2, \dots$, which are again interspersed with mixed patterns of the form $1^k (1^{k-1})^\ell$; see Fig. 10(b)–(f) and Fig. 11(a)–(f) for representative examples. (In fact, it follows from items (i) through (iii) above that the signatures 1^k and $1^k 1^{k-1}$ will dominate the mixed-mode dynamics of (1), with a transition that is roughly of the form $\dots \rightarrow 1^k \rightarrow 1^k 1^{k-1} \rightarrow 1^{k-1} \rightarrow \dots$, in accordance with our findings.) Finally, it is obvious from Fig. 12(a), (b) that the ‘highest’ 1^k -type pattern—at least with the chosen initial condition, and to the accuracy considered here—is achieved for $k = 8$, after which point pure SAO dynamics of type 0^1 takes over, in agreement with our claim that only a finite number of SAOs can occur in any given mixed-mode time series in (12).

Remark 6 Our numerics suggests that some variation in k_1 and k_3 does not qualitatively alter our conclusions on the mixed-mode dynamics of Eq. (1) as long as the condition $k_3 = \mathcal{O}(\varepsilon)$ is satisfied; examples can be found in Fig. 13(a) and (b).

While the above observations are of a qualitative nature, it is nevertheless possible to obtain some insight into the quantitative properties of the mixed-mode dynamics of Eq. (12) from our analysis. On the basis of Proposition 5, one can thus show that, for each $k \geq 1$ and ε sufficiently small, the width of the μ -interval corresponding to stable 1^k -type dynamics will be of the order $\mathcal{O}[\sqrt{\varepsilon}(-\ln \varepsilon)^{-\frac{1}{2}}]$. Specifically, approximating the integral term in Eq. (41) as in [14, Sect. 3.6], one finds

$$\Delta\mu^k = \frac{\underline{\mu}_k \kappa}{\sqrt{2} D_\mu} \frac{\sqrt{\varepsilon}}{\sqrt{-\ln \varepsilon}} [\ln(\sqrt{-\ln \varepsilon}) + \mathcal{O}(1)].$$

Evaluating the above estimate for $k_1(=\kappa) = 0.35, \varepsilon = 0.1$, and $\mu = \mu^c$ and noting that $D_\mu = 0.86625(= \frac{693}{800})$ then, we obtain $\Delta\mu^k \approx 0.00545[0.41702 + \mathcal{O}(1)]$, which agrees well with the corresponding numerical values of $\Delta\mu^k$ of about 0.004 to 0.005 that were inferred visually by simulating Eq. (12) for varying values of μ , as above, and by recording the observed mixed-mode patterns. (The degree of agreement seems particularly encouraging given the ‘large’ value of $\varepsilon = 0.1$ considered here.) In sum, numerical simulation hence suggests that the μ -interval on which the mixed-mode dynamics of Eq. (12) unfolds is approximately given by $(\underline{\mu}, \bar{\mu}) \approx (0.0465, 0.1125)$, which implies, in particular, $\Delta\mu \approx 0.0660$. Finally, it is worth noting that our numerical estimates for $\underline{\mu}$ and $\bar{\mu}$ satisfy $\mu^H < \underline{\mu} < \bar{\mu} < \mu^c$, as predicted. (Here, μ^H and μ^c are defined as at the beginning of Sect. 3.)

The parameter regime considered in this article motivated a simple scaling of k_3 with ε ; in fact, we set $k_3 = \varepsilon$. More generally, however, one could interpret k_3 —or even $k_1 k_3$ —as

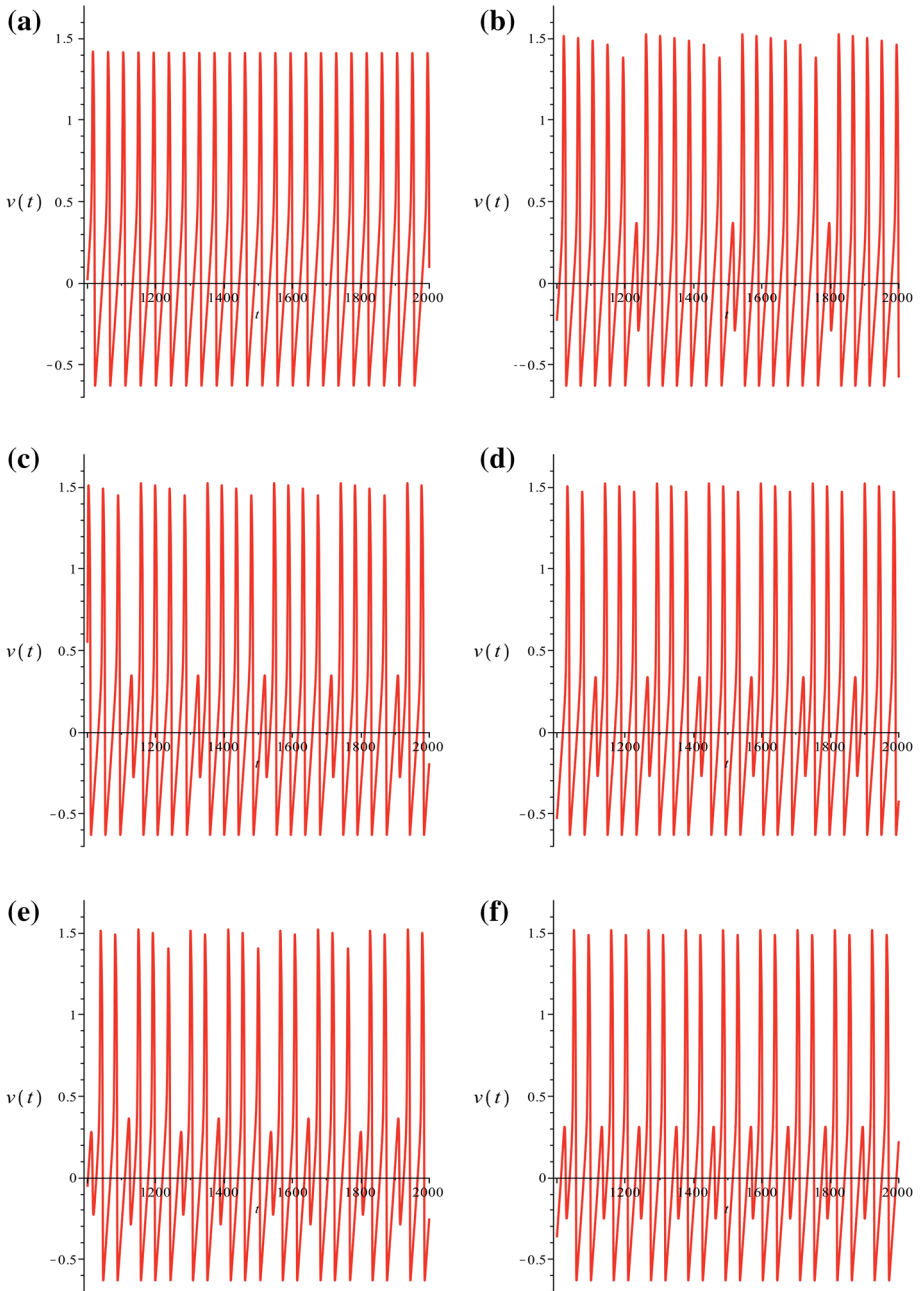


Fig. 9 Mixed-mode dynamics of Eq. (12) for varying values of μ . **a** $\mu = 0.1125: 1^0$, **b** $\mu = 0.11: 6^1$, **c** $\mu = 0.1075: 4^1$, **d** $\mu = 0.105: 3^1$, **e** $\mu = 0.1025: 3^1 2^1$, **f** $\mu = 0.1: 2^1$

an effective small parameter that is independent of ε ; correspondingly, Eq. (6) could then be studied as a true two-parameter singular perturbation problem. While geometric singular perturbation theory [6, 10] has matured as a field, however, the mathematics of such

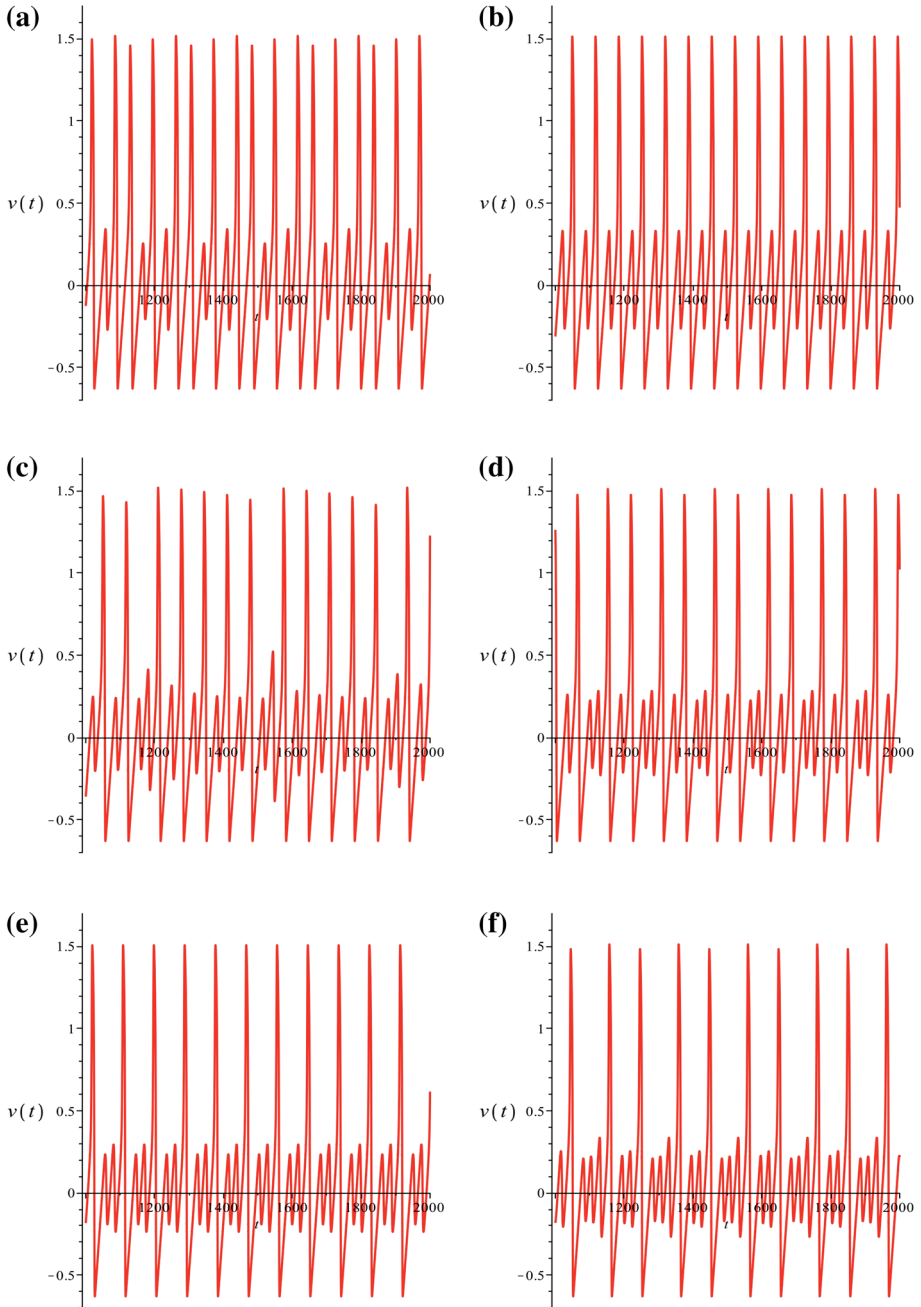


Fig. 10 Mixed-mode dynamics of Eq. (12) for varying values of μ . **a** $\mu = 0.095: 2^1 1^1$, **b** $\mu = 0.09: 1^1$, **c** $\mu = 0.085: 1^2 (1^1)^4$, **d** $\mu = 0.08: 1^2 1^1$, **e** $\mu = 0.075: 1^2$, **f** $\mu = 0.07: 1^3 1^2$

problems remains rudimentary; hence, we decided not to pursue that line of enquiry here. Still, further investigation into whether our results can be extended accordingly seems warranted, as preliminary analysis has revealed interesting dynamics in a similar generalisation

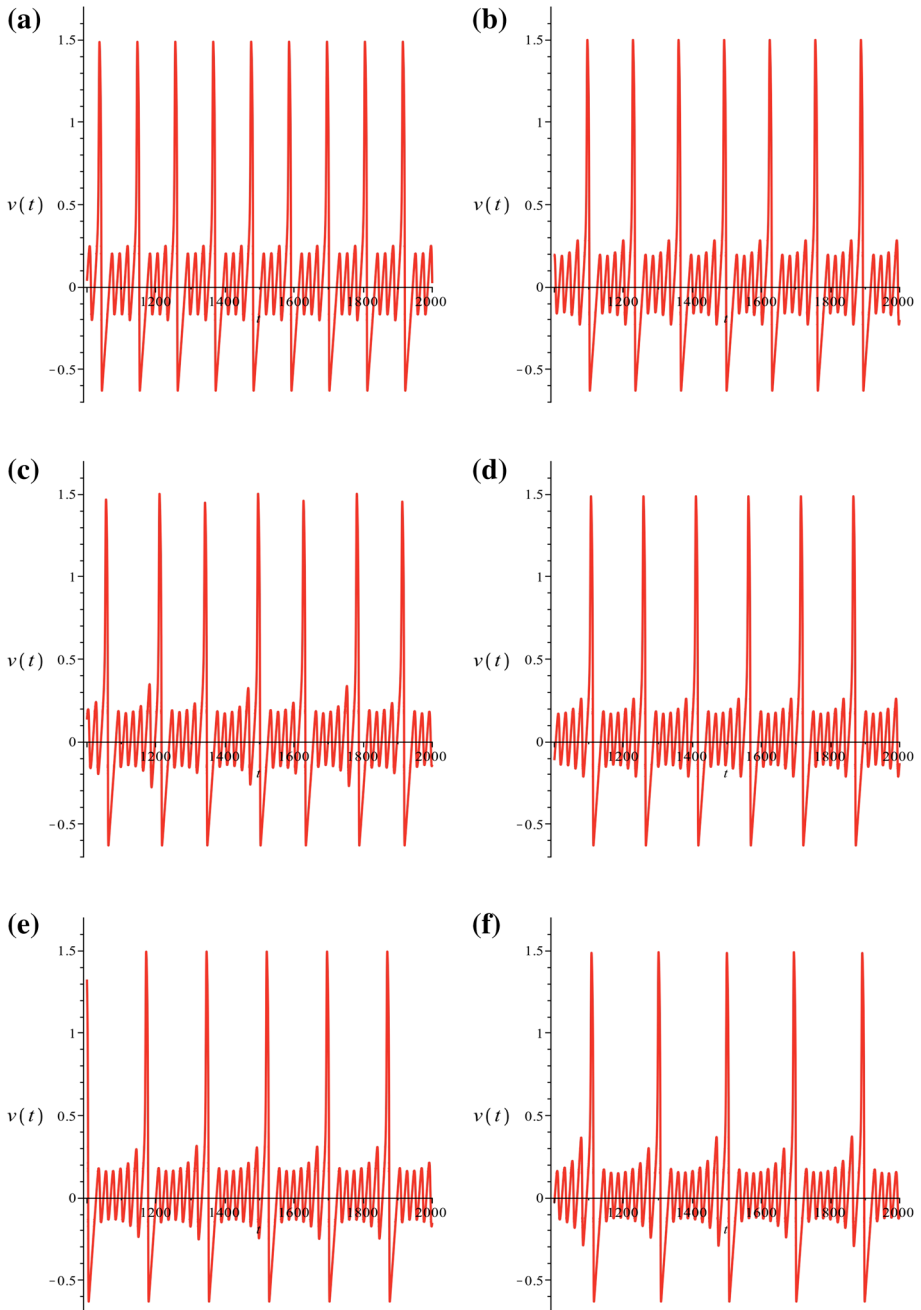


Fig. 11 Mixed-mode dynamics of Eq. (12) for varying values of μ . **a** $\mu = 0.065: 1^3$, **b** $\mu = 0.06: 1^4$, **c** $\mu = 0.0575: 1^5$, **d** $\mu = 0.055: 1^5$, **e** $\mu = 0.0525: 1^6$, **f** $\mu = 0.05: 1^7$

of the canonical Eq. (2). In particular, co-existence of mixed-mode oscillatory behaviour and delayed passage through Hopf bifurcation [13] has been observed, and will be elaborated on in an upcoming publication. Intuitively, such dynamics is due to a change in the strength of

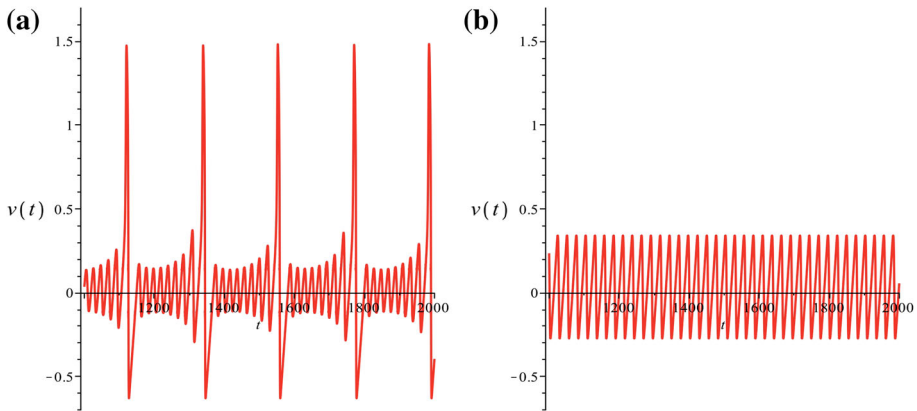


Fig. 12 Mixed-mode dynamics of Eq. (12) for varying values of μ . **a** $\mu = 0.0475: 1^8$, **b** $\mu = 0.0465: 0^1$

the global return mechanism: when $\varepsilon = \mathcal{O}(k_3)$, w is not necessarily reset to a neighbourhood of the strong canard Γ_ε ; rather, the corresponding return point may lie well away from the folded equilibrium P^+ in that case.

Remark 7 We note that we chose to fix the parameter k_1 , rather than to scale it with ε , as was also done in [17]—in spite of the fact that $k_1 = \mathcal{O}(\sqrt{\varepsilon})$. That choice complicates our analysis slightly, as it necessitates a correction to the return map $\bar{\Pi}$ in the fold region that was not present in [14]; recall the proof of Proposition 1. However, it seems in keeping with the assumptions made in [17].

The ‘folded saddle-node of type II’ [19] uncovered in Eq. (1) has also been studied in connection with a so-called ‘singular Hopf bifurcation;’ see [8] and the references therein for details. Roughly speaking, such bifurcations are observed in an ε -neighbourhood of a fold curve (for sufficiently small values of ε), and have been suggested as an alternative mechanism for generating mixed-mode dynamics; the relationship between folded saddle-node equilibria and singular Hopf bifurcation has been investigated in detail in [2]. In our case, it is straightforward to show that (1) has an equilibrium point at $P^* = (x_*, y_*, z_*)$, with $y_* = z_* = -\frac{1}{2}x_*(1 - x_*^2)$; following the procedure outlined in [8, Sect. 3.1], one can verify that P^* undergoes a Hopf bifurcation if the characteristic polynomial of the corresponding Jacobian,

$$\begin{aligned} &\lambda^3 + \frac{1}{\varepsilon}[\varepsilon k_1(1 + k_3) - (1 - 3x_*^2)]\lambda^2 + \frac{1}{\varepsilon}[\varepsilon k_1^2 k_3 + (1 - k_1 + 3k_1 x_*^2)(1 + k_3)]\lambda \\ &\quad + \frac{1}{\varepsilon}k_1 k_3 [2 - k_1(1 - 3x_*^2)] \\ &\equiv \lambda^3 + a_2(x_*, k_1, k_3, \varepsilon)\lambda^2 + a_1(x_*, k_1, k_3, \varepsilon)\lambda + a_0(x_*, k_1, k_3, \varepsilon) = 0, \end{aligned}$$

satisfies $a_1 > 0$ and $a_1 a_2 = a_0$. The former condition holds in the parameter regime considered here, while the latter is met for the unique value $x_H \approx 0.56801$ of $x_* \equiv x_*(k_1, k_3, \varepsilon)$. Finally, solving for the corresponding B_0 -value in (1), we find $B_0^H \approx 0.50067$ which, incidentally, is equivalent to the value for μ^H obtained in Sect. 3, in the context of (11). (Similarly, one can show that the critical μ -value μ^c defined in Sect. 2.4 corresponds to $B_0^c = 0.26\sqrt{3} \approx 0.45488$ and, hence, that the mixed-mode dynamics of the three time-scale Bonhoeffer–van der Pol oscillator will unfold approximately over the interval (B_0^c, B_0^H) .)

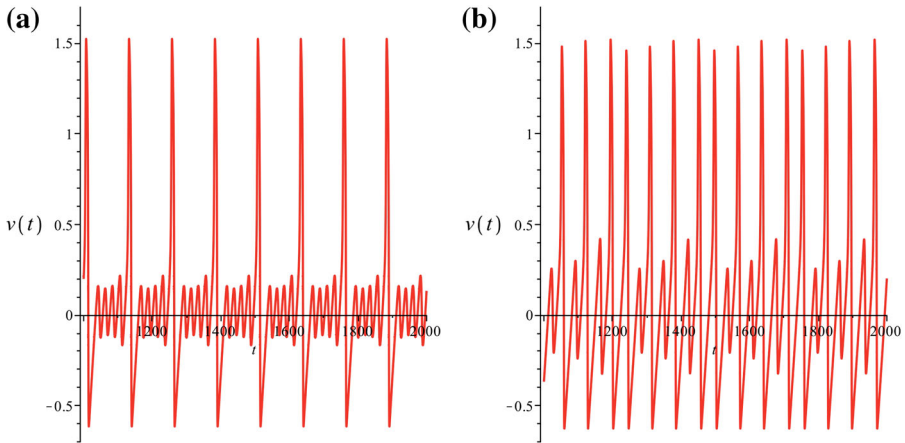


Fig. 13 Effect of varying k_1 and k_3 on the dynamics of Eq. (12). **a** $k_1 = 0.5, k_3 = 0.1,$ and $\mu = 0.075: 2^4$, **b** $k_1 = 0.35, k_3 = 0.05,$ and $\mu = 0.110: 2^1(1^1)^2$

Since, however, the asymptotics obtained in this article is, by definition, only valid in an ‘intermediate’ μ -regime—away from both ‘pure’ SAO and LAO dynamics—we do not consider mixed-mode behaviour that may be induced by a singular Hopf bifurcation in (1).

While our analysis is mostly precise, as we have systematically accounted for the orders of any terms omitted in the process, a fully rigorous study would have to rely on the ‘blow-up’ technique, or geometric desingularisation [5, 12]. In fact, the discussion in Sect. 3.1 could equally be recast in terms of a ‘rescaling’ chart that covers the fold region and two ‘phase-directional’ charts which describe the entry and exit mechanisms, respectively, as is routinely done in the application of blow-up; see again [5, 12] for but two examples. However, in the interest of keeping our presentation accessible, and in following [14] and [15], we have opted to formulate our results in terms of equivalent coordinate rescalings and projectivisations, and thereby to sacrifice some rigour.

Our approach has its inherent limitations, of course: thus, for instance, the asymptotics of the return map Π derived in Sect. 3—as well as of its one-dimensional reduction Φ —breaks down at the boundaries between sectors of rotation; see [14, Sect. 4] for details. While we have hence excluded a neighbourhood of the corresponding secondary canards Γ_ε^j from our analysis, it is there that complicated mixed-mode patterns can arise due to ‘jumps’ between non-adjacent sectors and period-doubling bifurcation, both of which may yield chaotic dynamics. In fact, the proof of Proposition 1 already assumes that the flow of Eq. (14) stays away from the strong canard Γ_ε , which is reflected in our assumption that $h = \mathcal{O}(\varepsilon^M)$ is small, but not exponentially so. Dynamics resulting from a violation of that condition is illustrated in Fig. 14, where a stable mixed-mode pattern is shown to co-exist with a canard cycle undergoing period doubling; the latter is realised for initial w -values close to the ‘critical’ value $w_0^c = \sqrt{\varepsilon} \bar{w}_0^c$ of w , with \bar{w}_0^c defined as in (35), which implies that the corresponding h -value must be near-exponentially small.

Period-doubling in the extended Bonhoeffer–van der Pol oscillator has been studied in detail in [7]; in the process, the mixed-mode dynamics that is generated upon variation of the two parameters k_3 and B_0 was described numerically in a number of regimes, down to $k_3 = 0.2$. However, and in contrast to standard convention, mixed-mode patterns were organised in terms of ‘isospike diagrams,’ i.e., distinguished in terms of the total number of ‘spikes’ within a period, rather than their signature L^k ; interestingly, it was shown that the

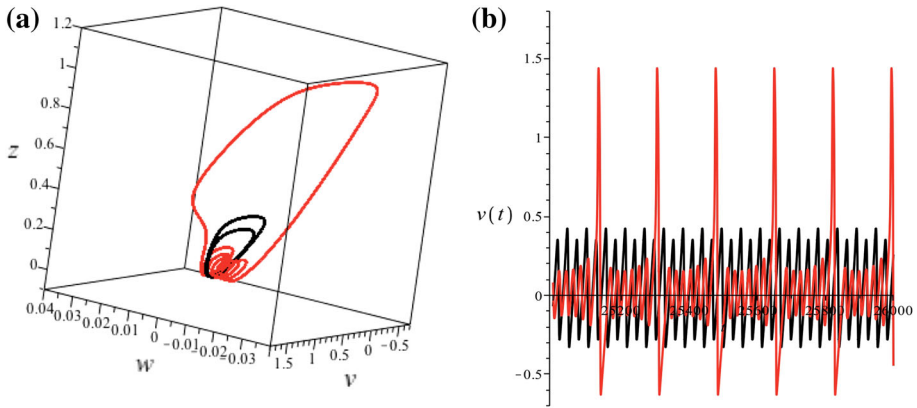


Fig. 14 Co-existence of type-1⁶ MMO (red) and canard cycle after period doubling (black) for $\mu = 0.051$. **a** Orbits in (v, z, w) -space, **b** Time series of $v(t)$

underlying hierarchical structure is well-represented by a Stern-Brocot tree, instead of the Farey tree which is usually invoked in that context. In particular, and in agreement with [17], period-doubling cascades were found to be interspersed with chaotic phases which unfold over very narrow B_0 -intervals; the latter may well correspond to the boundaries between our sectors of rotation. Further investigation is necessary to establish fully how their results relate to those obtained in this article.

Finally, in a recent study by Shimizu et al. [18], the dynamics of a modification of Eq. (1) was considered subject to a weak periodic perturbation close to Hopf bifurcation. In analogy to the approach developed here, a one-dimensional reduction was obtained for the return map that is induced by the resulting flow; however, that reduced map was not found to be unimodal, as in our case, but circle-like. A novel type of bifurcation, termed ‘MMO-incrementing bifurcation’ (MMOIB), was reported by the authors; moreover, highly complex, intermittently chaotic mixed-mode patterns that include rare bursts over long time intervals were observed in the corresponding time series. It would seem worthwhile to explore whether the geometric framework applied in this article can be extended to the modified Bonhoeffer-van der Pol oscillator studied in [18].

Acknowledgments The authors’ research was supported by the Research Foundation Flanders (FWO) under grant number G.0939.10N. Moreover, E. K. acknowledges support from the Polish Ministry of Science and Higher Education.

References

1. Brøns, M., Krupa, M., Wechselberger, M.: Mixed mode oscillations due to the generalized canard phenomenon. In: *Bifurcation Theory and Spatio-Temporal Pattern Formation*, vol. 49 of Fields Institute Communications, pp. 39–63. American Mathematical Society, Providence, RI, (2006)
2. Curtu, R., Rubin, J.: Interaction of canard and singular Hopf mechanisms in a neural model. *SIAM J. Appl. Dyn. Syst.* **10**(4), 1443–1479 (2011)
3. Desroches, M., Guckenheimer, J., Krauskopf, B., Kuehn, C., Osinga, H.M., Wechselberger, M.: Mixed-mode oscillations with multiple time scales. *SIAM Rev.* **54**(2), 211–288 (2012)
4. Dumortier, F.: Techniques in the theory of local bifurcations: blow-up, normal forms, nilpotent bifurcations, singular perturbations. In: *Bifurcations and Periodic Orbits of Vector Fields* (Montreal, PQ, 1992), vol. 408 of NATO Adv. Sci. Inst. Ser. C Math. Phys. Sci., pp. 19–73. Kluwer Academic Publisher, Dordrecht (1993)

5. Dumortier, F., Roussarie, R.: Canard cycles and center manifolds. *Mem. Am. Math. Soc.* **121**(577), 1–100 (1996) (With an appendix by Cheng Zhi Li)
6. Fenichel, N.: Geometric singular perturbation theory for ordinary differential equations. *J. Differ. Equ.* **31**(1), 53–98 (1979)
7. Freire, J.G., Gallas, J.A.C.: Stern-Brocot trees in cascades of mixed-mode oscillations and canards in the extended Bonhoeffer–van der Pol and the Fitzhugh–Nagumo models of excitable systems. *Phys. Lett. A* **375**, 1097–1103 (2011)
8. Guckenheimer, J.: Singular Hopf bifurcation in systems with two slow variables. *SIAM J. Appl. Dyn. Syst.* **7**(4), 1355–1377 (2008)
9. Izhikevich, E.M.: *Dynamical Systems in Neuroscience: The Geometry of Excitability and Bursting*. Computational Neuroscience. MIT Press, Cambridge, MA (2007)
10. Jones, C.K.R.T.: Geometric singular perturbation theory. In: *Dynamical Systems (Montecatini Terme, 1994) Lecture Notes in Mathematics*, vol. 1609, pp. 44–118. Springer, Berlin, (1995)
11. Koper, M.T.M.: Bifurcations of mixed-mode oscillations in a three-variable autonomous van der Pol–Duffing model with a cross-shaped phase diagram. *Phys. D* **80**(1–2), 72–94 (1995)
12. Krupa, M., Szmolyan, P.: Extending geometric singular perturbation theory to nonhyperbolic points–fold and canard points in two dimensions. *SIAM J. Math. Anal.* **33**(2), 286–314 (2001)
13. Krupa, M., Wechselberger, M.: Local analysis near a folded saddle-node singularity. *J. Differ. Equ.* **248**(12), 2841–2888 (2010)
14. Krupa, M., Popović, N., Kopell, N.: Mixed-mode oscillations in three time-scale systems: a prototypical example. *SIAM J. Appl. Dyn. Syst.* **7**(2), 361–420 (2008)
15. Krupa, M., Popović, N., Kopell, N., Rotstein, H.G.: Mixed-mode oscillations in a three time-scale model for the dopaminergic neuron. *Chaos* **18**(1), 015106 (2008)
16. Olver, F.W.J.: *Asymptotics and Special Functions*. AKP Classics. A K Peters Ltd., Wellesley, MA, (1997). Reprint of the original [Academic Press, New York, 1974]
17. Sekikawa, M., Inaba, N., Yoshinaga, T., Hikiyama, T.: Period-doubling cascades of canards from the extended Bonhoeffer–van der Pol oscillator. *Phys. Lett. A* **374**(36), 3745–3751 (2010)
18. Shimizu, K., Yuto, S., Sekikawa, M., Inaba, N.: Complex mixed-mode oscillations in a Bonhoeffer–van der Pol oscillator under weak periodic perturbation. *Phys. D* **241**(18), 1518–1526 (2012)
19. Szmolyan, P., Wechselberger, M.: Canards in \mathbb{R}^3 . *J. Differ. Equ.* **177**(2), 419–453 (2001)
20. Szmolyan, P., Wechselberger, M.: Relaxation oscillations in \mathbb{R}^3 . *J. Differ. Equ.* **200**(1), 69–104 (2004)
21. Tu, S.T.: A phase-plane analysis of bursting in the three-dimensional Bonhoeffer–van der Pol equations. *SIAM J. Appl. Math.* **49**(2), 331–343 (1989)
22. Wechselberger, M.: Existence and bifurcation of canards in \mathbb{R}^3 in the case of a folded node. *SIAM J. Appl. Dyn. Syst.*, **4**(1), 101–139 (2005) (electronic)
23. Wilson, C.J., Callaway, J.C.: Coupled oscillator model of the dopaminergic neuron of the substantia nigra. *J. Neurophysiol.* **83**(5), 3084–3100 (2000)